SAND2018-9746R

International Collaboration on Spent Fuel Disposition in Crystalline Media: FY18 Progress Report

Fuel Cycle Research & Development

Prepared for
U.S. Department of Energy
Spent Fuel Waste Science & Technology

Yifeng Wang, Teklu Hadgu, Elena Kalinina,
Carlos Jove-Colon
Sandia National Laboratories
Boris Faybishenko
Lawrence Berkeley National Laboratory

August 22, 2018

Sandia National Laboratories is a multi-mission laboratory managed and operated by National Technology and Engineering Solutions of Sandia, LLC., a wholly owned subsidiary of Honeywell International, Inc., for the U.S. Department of Energy's National Nuclear Security Administration under contract DE-NA0003525.

FCT Quality Assurance Program Document

Appendix E
FCT Document Cover Sheet

Name/Title of Deliverable/Milestone	International Collaboration on Spent Fuel Disposition in Crystalline Media: FY18 Progress Report (M4SF-18SN010302092)
Work Package Title and Number	DR Crystalline Disposal R&D
Work Package WBS Number	FT-18SN010302029
Responsible Work Package Manager	Yifeng Wang (Name/Signature)

Date Submitted 8/22/2018

Quality Rigor Level for Deliverable/Milestone	☐ QRL-3	☐ QRL-2	☐ QRL-1 ☐ Nuclear Data	☒ N/A*

This deliverable was prepared in accordance with Sandia National Laboratories
(Participant/National Laboratory Name)

QA program which meets the requirements of
☒ DOE Order 414.1 ☐ NQA-1-2000

This Deliverable was subjected to:

☐ Technical Review

Technical Review (TR)
Review Documentation Provided
☐ Signed TR Report or,
☐ Signed TR Concurrence Sheet or,
☐ Signature of TR Reviewer(s) below
Name and Signature of Reviewers
N/A

☐ Peer Review

Peer Review (PR)
Review Documentation Provided
☐ Signed PR Report or,
☐ Signed PR Concurrence Sheet or,
☐ Signature of PR Reviewer(s) below

*Note: In some cases there may be a milestone where an item is being fabricated, maintenance is being performed on a facility, or a document is being issued through a formal document control process where it specifically calls out a formal review of the document. In these cases, documentation (e.g., inspection report, maintenance request, work planning package documentation or the documented review of the issued document through the document control process) of the completion of the activity along with the Document Cover Sheet is sufficient to demonstrate achieving the milestone. QRL for such milestones may be also be marked N/A in the work package provided the work package clearly specifies the requirement to use the Document Cover Sheet and provide supporting documentation.

INTERNATIONAL COLLABORATION ON SPENT FUEL DISPOSITION IN CRYSTALLINE MEDIA: FY17 PROGRESS REPORT

EXECUTIVE SUMMARY

Active participation in international R&D is crucial for achieving the Spent Fuel Waste Science & Technology (SFWST) long-term goals of conducting "experiments to fill data needs and confirm advanced modeling approaches" and of having a "robust modeling and experimental basis for evaluation of multiple disposal system options" (by 2020). DOE's Office of Nuclear Energy (NE) has developed a strategic plan to advance cooperation with international partners. The international collaboration on the evaluation of crystalline disposal media at Sandia National Laboratories (SNL) in FY18 focused on the collaboration through the Development of Coupled Models and their Validation against Experiments (DECOVALEX-2019) project. The DECOVALEX project is an international research and model comparison collaboration, initiated in 1992, for advancing the understanding and modeling of coupled thermo-hydro-mechanical-chemical (THMC) processes in geological systems. SNL has been participating in three tasks of the DECOVALEX project: Task A. Modeling gas injection experiments (ENGINEER), Task C. Modeling groundwater recovery experiment in tunnel (GREET), and Task F. Fluid inclusion and movement in the tight rock (FINITO). FY18 work focused on Task C and preparing the interim reports for the three tasks SNL has been imvolved. The major accomplishments are summarized below:

- *Task A. Modeling gas injection experiments (ENGINEER):* Bentonite has been proposed as a buffer material for a deep geologic repository. Understanding gas migration in compacted clay materials is important for a performance assessment of an engineered barrier system of a repository system. Existing data demonstrate the complexity of gas migration in such low-permeability materials. Through a time-series analysis of outflow rate, we show that gas migration in water saturated compacted clay material exhibits a typical deterministic chaotic behavior. The dimension of the system ranges from 3 to 4. The dynamic behavior of the system has been shown closely related to clay matrix dilation, fracturing and fracture healing as induced by gas bubble movement. The concept proposed here provide a new perspective for modeling gas migration in low-permeability materials.
- *Task C. Modeling groundwater recovery experiment in tunnel (GREET):* The task uses the data collected in a research tunnel at 500 m depth, at the Japan Atomic Energy Agency (JAEA) Mizunami Underground Research Laboratory (MIU), to understand the hydrological-mechanical-chemical environment. The model analysis conducted in FY18 has demonstrated a general approach to developing a small-scale discrete fracture network model around the Research tunnel. The data used included fracture traces mapped on the tunnel walls, fractures observed in borehole 12MI33, packer test results in 6 test intervals of borehole 12MI33, and measured inflow into the different segment of the Research tunnel during the tunnel excavation. The discrete fracture network (DFN) model includes:
    a. The fractures observed in the Research tunnel and borehole 12MI33. These fractures have deterministic locations and stochastic (radius, permeability, and aperture) properties derived from the fracture analysis.
    b. Stochastic fractures (the location changes with each realization) generated based on the fracture size, orientation, intensity, and properties derived from the fracture analysis.

  The discrete fracture network model was then upscaled to a continuum model to be used in flow simulations. A flow model was developed centered on the research tunnel, and using a highly refined regular mesh. In this study development and utilization of the model is presented. The modeling analysis used permeability and porosity fields from the discrete fracture network model as well as a homogenous model using fixed values of permeability and porosity. The simulations were designed to reproduce hydrology of the modeling area and to predict inflow of water into

the research tunnel during excavation. Modeling results were compared with the project hydrology data. Successful matching of the experimental data was obtained for simulations based on the discrete fracture network model.

- *Task F. Fluid inclusion and movement in the tight rock (FINITO):* Fluid inclusions can be found within mineral crystals or along grain boundaries in all types of sedimentary rocks. For a long-term performance assessment of a geologic repository, it is important to characterize the distribution, amount and interconnectivity of fluid inclusions in the host rock and to predict migration of these inclusions after waste emplacement. Task F is designed to gain mechanistic understanding of possible physical processes involved in fluid inclusion migration in tight rocks such as rock salt, with an ultimate goal to develop robust, predictive THMC modeling tools for a long-term performance assessment of a deep geologic repository in such media. The task will leverage the data provided by BGR, Germany. In fiscal year 2018, the work at SNL has refined the model for individual fluid inclusion migration in rock salt. The model developed can qualitatively explain a number of key features of experimental observations. Specifically, the model can predict: (1) a linear increase in migration evelocity with increasing thermal gradient, (2) a nonlinear increase in migration velocity with inclusion size, (3) an overall aceleration in fluid migration with temperature, (4) the dependence of migration velocity on mechanical loadings. A preliminary analysis for biphase fluid inclusions has also been performed. A bifurcation point in vapor/liquid volume ratio for the direction of fluid migration is derived.

Future work will include the development of a full model for gas migration in clay materials and fluid inclusion migration in salt. For Task C, more comprehensive modeling simulations will be conducted on fluid inflow and chemical reactions. For all three tasks, model simulation results will be closely compared to experimental and field data.

1. OBJECTIVES

Recognizing the benefits of international collaboration in the common goal of safely and efficiently managing the back end of the nuclear fuel cycle, DOE's Office of Nuclear Energy (NE) and its office for Spent Fuel Waste Science & Technology (SFWST) have developed a strategic plan to advance cooperation with international partners (Birkholzer et al., 2013; UFD, 2012). The plan lays out two interdependent areas of international collaboration. The first area is cooperation with the international nuclear community through participation in international organizations, working groups, committees, and expert panels. Such participation typically involves conference and workshop visits, information exchanges, reviews, and training and education. The second area of international collaboration is active R&D participation of U.S. researchers within international projects or programs (UFD, 2012). By active R&D, it is meant that U.S. researchers work closely together with international scientists on specific R&D projects relevant to both sides. With respect to geologic disposal of radioactive waste, such active collaboration provides direct access to information, data, and expertise on various disposal options and geologic environments that have been collected internationally over the past decades. Many international programs have operating underground research laboratories (URLs) in clay/shale, granite, and salt environments, in which relevant field experiments have been and are being conducted. Depending on the type of collaboration, U.S. researchers can participate in planning, conducting, and interpreting experiments in these URLs, and thereby get early access to field studies without having in situ research facilities in the United States.

The DOE also considers this second area, active international R&D, to be very beneficial in achieving the program's long-term goals of conducting "experiments to fill data needs and confirm advanced modeling approaches" and of having a "robust modeling and experimental basis for evaluation of multiple disposal system options" (by 2020). Advancing opportunities for active international collaboration with respect to geologic disposal has therefore been the primary focus of SFWST's international strategy in the recent year (Birkholzer et al., 2013; Birkholzer, 2012).

This report summarizes the work accomplished in FY18 at Sandia National Laboratories (SNL) related to international collaborations on the evaluation of crystalline rocks as disposal media. The FY18 work focused on the collaboration through the Development of Coupled Models and their Validation against Experiments (DECOVALEX-2019) project. The DECOVALEX project is an international research and model comparison collaboration, initiated in 1992, for advancing the understanding and modeling of coupled thermo-hydro-mechanical-chemical (THMC) processes in geological systems. SNL has been participating in three tasks of the DECOVALEX project: Task A. Modeling gas injection experiments (ENGINEER), Task C. Modeling groundwater recovery experiment in tunnel (GREET), and Task F. Fluid inclusion and movement in the tight rock (FINITO). This work directly supports the following SFWST objectives:

- Develop a fundamental understanding of disposal system performance in a range of environments for potential wastes that could arise from future nuclear fuel cycle alternatives through theory, simulation, testing, and experimentation.
- Develop a computational modeling capability for the performance of storage and disposal options for a range of fuel cycle alternatives, evolving from generic models to more robust models of performance assessment.

The work documented here also addresses the following specific topics identified based on the SFWST R&D Implementation Plan (Wang, 2014).

- Topic #S5: Evaluation of state of the art of site characterization techniques
- Topic #S7: Identification of the needs for using underground research laboratory
- Topic #P1: Development of discrete fracture network model

- Topic #P2: Parameter estimation and uncertainty quantification of field testing

1.1 REFERENCES

Birkholzer, J.T. (2012). Status of UFD Campaign International Activities in Disposal Research. Report prepared for U.S. Department of Energy Used Fuel Disposition Campaign, FCRD-UFD-2012-000295.

Birkholzer, J., Asahina, D., Chen, F., Gardner, P., Houseworth, J., Jove-Colon, C., Kersting, A., Nair, P., Nutt, M., Li, L., Liu, H.H., Painter, S., Reimus, P., Rutqvist, J., Steefel, C., Tynan, M., Wang, Y., Zavarin, M. (2013). An overview of US disposal research activities linked to international URLs. Proceedings of the 2013 International High-Level Radioactive Waste Management Conference (IHLRWM), April 28 – May 2, 2013, Albuquerque, New Mexico.

UFD (2012). Office of Used Fuel Disposition International Program — Strategic Plan (2013) April 2012, U.S. Department of Energy.

Wang, Y. (2014) Used Fuel Disposal in Crystalline Rocks: Status and FY14 Progress, FCRD-UFD-2014-000060.

2. FLUID INCLUSION AND MOVEMENT IN THE TIGHT ROCK (FINITO)

2.1 INTRODUCTION

Fluid inclusions containing liquid, gas or both phases can be found within mineral crystals (intra-crystalline) or along grain boundaries (inter-crystalline) in all types of sedimentary rocks (Roedder,1984; Ghanbaradeh et al., 2015). They were formed under various pressure and temperature conditions during the genesis. The size of fluid inclusions ranges several micrometres to millimeters and are usually invisible in detail without a microscope. These fluid inclusions are usually dispersed in a very low concentration but can form local accumulations in a rock volume up to some cubic meters.

The initial fluid inclusions in undisturbed rock are situated under a lithostatic pressure, which is much higher than a corresponding hydrostatic pressure in deep subsurface. Because of the low rock permeability, the migration of such fluids is almost impossible even under a high pressure-gradient condition. Fluid release from crystals will take place if the stress state changes. In case of a drilling or an excavation, stress will be redistributed, resulting in a deviatoric stress state. If fluid pressure is higher than the minimal principal stress, dilatancy-controlled fluid migration occurs. This results in the generation of micro-fissures between crystal structures with an increased permeability. With regard to the long-term performance of a potential geologic repository, it is important to characterize the distribution, amount and interconnectivity of the fluid inclusions. It is also important to determine the permeability of micro-fissures and to characterize the hydraulic properties after the fluid release.

Understanding relevant underlying processes and developing appropriate model concepts are essential in this task. Modelling of the measured data needs a comprehensive effort, because a quantitative measurement at a microscale is not possible. An upscaling process from a microscale consideration to a macroscale observation is necessary.

In the construction phase of a geologic repository, coupled hydrologic-mechanical (HM) processes are important, while in the post-closure phase, coupled thermal-hydrologic-mechanical (THM) processes should be considered. In addition, chemical reactions and mineralogical alterations, especially under high temperature conditions, are indispensable to the full understanding of the system. The emphasis of this task is to gain understanding of possible physical processes involved in fluid inclusion migration in tight rocks such as rock salt or shale, with an ultimate goal to develop robust, predictive thermal-hydrologic-mechanical-chemical (THMC) modeling tools for a long-term performance assessment of a deep geologic repository.

2.2 EXPERIMENTAL DATA

Extensive microscopic study on the core structure using e.g. laser microscope, Computer tomography, electron backscatter diffraction (EBSD) is available which may help in description of the morphology of the pore space and construction of numerical mesh for the pore scale simulation. In addition, there are data about pressure, flow and geochemical components from more than 20 boreholes from underground laboratories, which allow us to understand mechanical, hydraulic and geochemical processes (Hammer et al., 2013). Most of these data are provided by Federal Institute for Geosciences and Natural Resources (BGR), Germany.

2.3 PLAN FOR TASK CASE STUDY

Two cases are defined and will be qualitatively studied.

Case 1: Fluid migration due to excavation

In the operating phase of a repository, in a tight rock such as salt, embedded fluid inclusions may begin to move due to stress redistribution around the excavation and reopening of the micro-fissure and crystal boundary. The model system for this case is shown in Figure 2-1. We assume there is a fluid-inclusion in the tight rock located somewhere in a two-dimensional domain (10X10 m) constrained by an isotropic stress state of 25 MPa, indicating a depth of 1000 m below the surface. A hole with a diameter of 0.8 m will be drilled in the middle of the domain. Due to the excavation, fluid, may consist of two (gaseous and liquid) phase, begins to move towards to tunnel. Numerical tools are therefore needed to determine:

- the time-dependent stress redistribution due to mechanical creeping
- the zone with micro-fissure according to the dilatancy-criterion
- the shortest distance between the fluid inclusion and the drilled hole, which may induce to the movement of the fluid
- the percolation threshold for the fluid movement (capillary pressure, surface tension between three phases, minimal principal stress state).

In this case, a two-phase flow model coupled with a mechanical model (elastic, plastic and even creep model) is needed to analyze different scenarios even at the pore-scale domain.

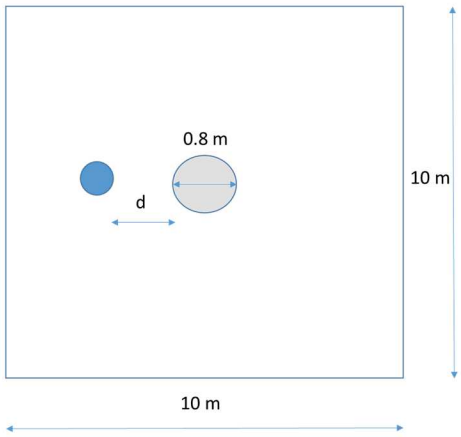

Figure 2-1: A single fluid inclusion located in a 2D domain with a hole.

Case 2: Fluid movement due to heating

In the closure phase of a repository, after the emplacement of the backfill, the stress state is approaching to the initial state. The micro-fissure will be healed again. However, under the high temperature conditions (100 – 200 °C) (Figure 2-2), thermal expansion of fluid and solid lead to volume increase. Due to the solubility difference, embedded fluid inclusions may move toward or away from a heating source (Figure 2-3).

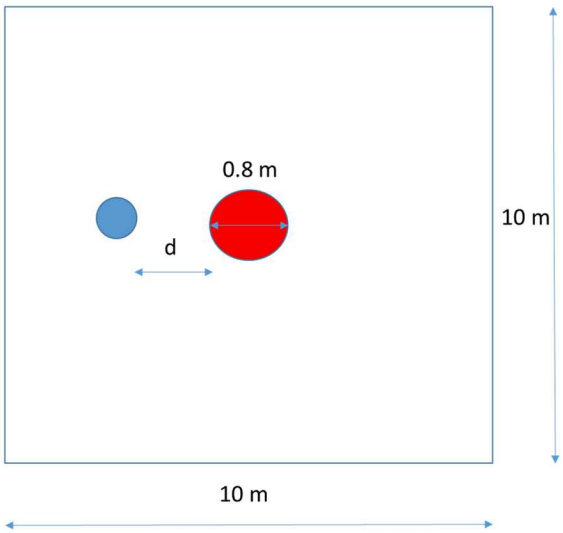

Figure 2-2: A single fluid inclusion located in a 2D domain with a heated domain.

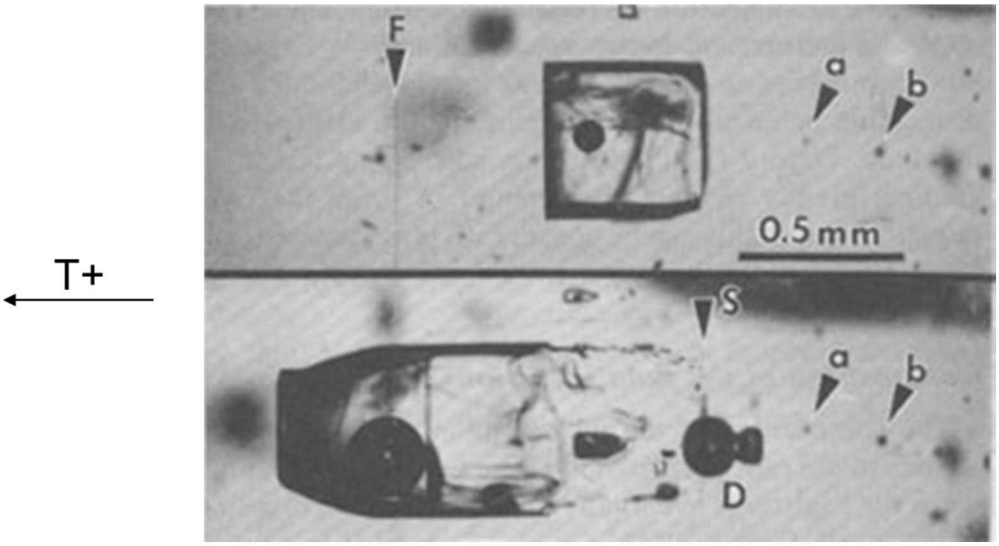

Figure 2-3: Experimental observation on fluid-migration after 156-hour run at 202°C ambient and 1.5°C/cm gradient (Roedder, 1984):

For this case, a coupled thermal-hydro-chemical model should be developed to consider all possible processes including:

- Mineral dissolution and precipitation on with a fluid inclusion
- Dihedral angle changes of fluid inclusion at grain boundaries,
- Thermal deformation,
- Induced porosity change and
- Related permeability change.

2.4 SCHEDULE

The master plan of the task includes three work packages with the focus on the understanding of the coupled thermal-hydro-mechanical and chemical processes involved in the system:

WP - 1: Literature study and process definition
WP - 2: Upscaling from microscale to macroscale basis
WP - 3: Model development and against observations

		2016		2017		2018		2019
	1 WS	2 WS	3 WS	4 WS	5 WS	6 WS	7 WS	8 WS
WP - 1								
Literature Recherche & Data Analyse								
Process Definition/Description								
Conceptuel Modeling								
WP - 2								
Upscalling Study (microscale - macroscale)								
Mathematical Formulation								
Programm Developement/Implement								
WP - 3								
Modelling against Observation								

2.5 MATHEMATICAL FORMULATION OF FLUID INCLUSION MIGRATION UNDER A THERMAL GRADIENT

In fiscal year 2017, the work at Sandia National Laboratories (SNL) has focused on the model formulation of an individual fluid inclusion in rock salt. A number of experimental and modelling studies have been conducted on fluid inclusion migration in salt (Anthony and Cline, 1971, 1972; Olander et al., 1981; Yagnik, 1983). A reasonable model should be able to account for the following key features of fluid inclusion migration observed experimentally (Figure 2-4):

- A liquid fluid inclusion moves toward a heating source at a velocity linearly proportional to the thermal gradient imposed (Figure 2-4A). Interestingly, it seems that the migration velocity also depends on a mechanical loading. Increasing the mechanical loading enhances migration.
- The velocity of inclusion migration also increases with the size of the inclusion, but not linearly (Figure 2-4B). The velocity appears to reach a plateau as the size of the inclusion further increases. This plateau seems to shift to a higher value at a higher temperature. This shift becomes more pronounced for small inclusions.

A

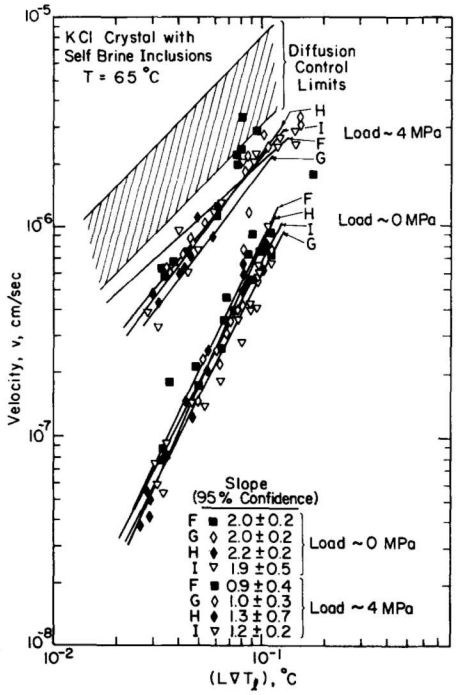
KCl Crystal with
Self Brine Inclusions
T = 65 °C
Diffusion
Control
Limits
Load ~ 4 MPa
Load ~ 0 MPa
Velocity, v, cm/sec
Slope
(95% Confidence)
F ■ 2.0±0.2
G ◊ 2.0±0.2
H ♦ 2.2±0.2
I ▽ 1.9±0.5
Load ~ 0 MPa
F ■ 0.9±0.4
G ◊ 1.0±0.3
H ♦ 1.3±0.7
I ▽ 1.2±0.2
Load ~ 4 MPa
(L∇T), °C

B

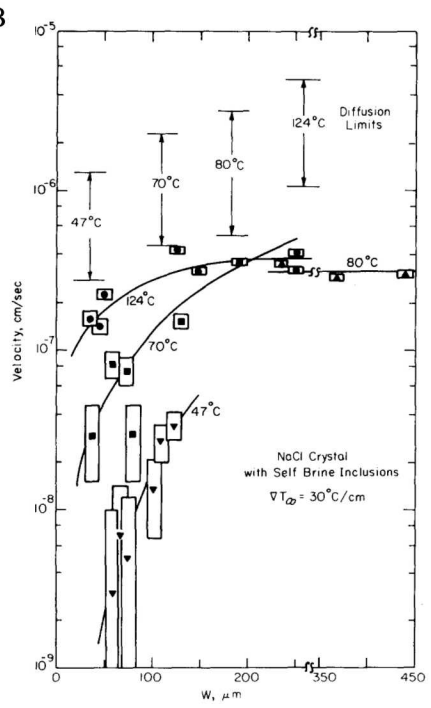
Diffusion
Limits
124°C
80°C
70°C
47°C
Velocity, cm/sec
NaCl Crystal
with Self Brine Inclusions
W, μm

C

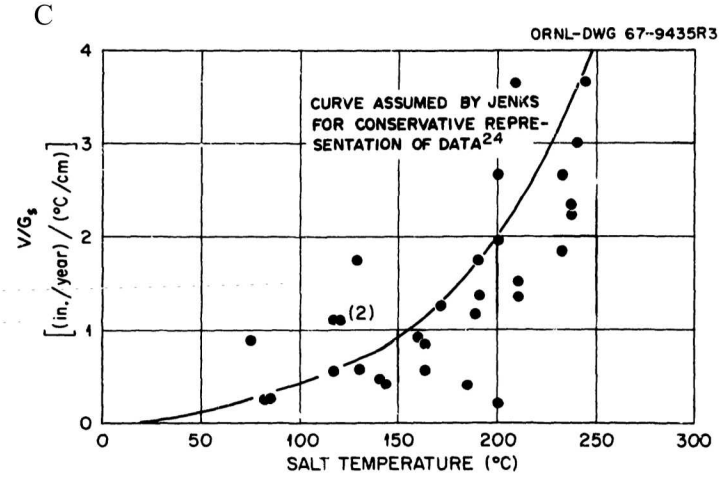
ORNL-DWG 67-9435R3
CURVE ASSUMED BY JENKS
FOR CONSERVATIVE REPRE-
SENTATION OF DATA[24]
V/Gs
[(in./year) / (°C/cm)]
(2)
SALT TEMPERATURE (°C)

D

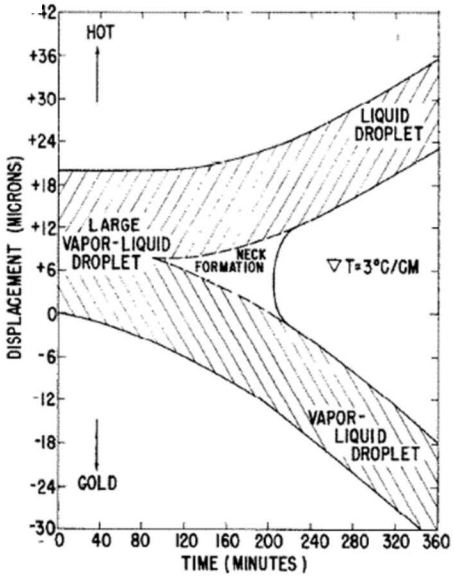
HOT
LIQUID
DROPLET
LARGE
VAPOR-LIQUID
DROPLET
NECK
FORMATION
∇T=3°C/CM
VAPOR-
LIQUID
DROPLET
COLD
DISPLACEMENT (MICRONS)
TIME (MINUTES)

E

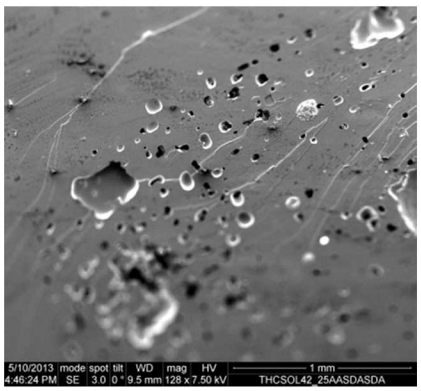
5/10/2013 mode spot tilt WD mag HV 1 mm
4:46:24 PM SE 3.0 0 ° 9.5 mm 128 x 7.50 kV THCSOL42_25AASDASDA

F

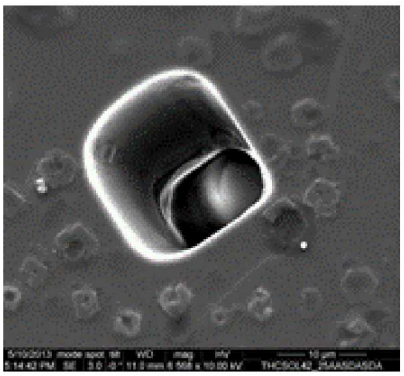

Figure 2-4: Key features of fluid inclusion migration under a thermal gradient. A – C: Migration velocity of liquid inclusion as a function of temperature gradient, inclusion size, and temperature (Olander et al., 1982; Jenk, 1979). D: Liquid-dominated inclusions migrate upward the thermal gradient while vapour-dominated inclusions move downward the gradient (Anthony and Cline, 1972); E-F: Channelling of an advancing front of a moving fluid inclusion (F. Caporuscio, per. Comm.), indicating the morphologic instability of the front.

- The velocity of fluid inclusion migration increases approximately exponentially with the overall temperature (Figure 2-4C).
- Complex behaviours have been observed for biphase inclusions. Liquid-dominated inclusions migrate upward the thermal gradient while vapour-dominated inclusions move downward the gradient (Figure 2-4D). Therefore, there is a bifurcation point in a vapour/liquid ratio for the direction of inclusion movement.
- As a fluid inclusion migrate along a thermal gradient, its shape may change and it may break into smaller inclusions (Yagnik, 1983). Remarkably, at the advancing front of an inclusion, channelling may be developed, indicating morphologic instability of the front (Figures 2-4E and 2-4F).

To account for these feature, we have formulated the following dynamic model for a single fluid inclusion migration in a thermal gradient field.

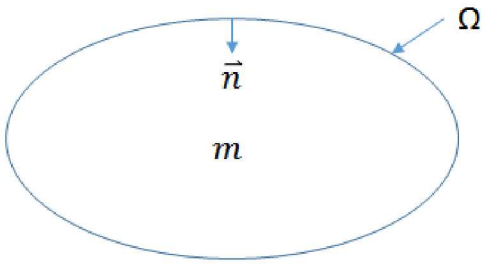

Figure 2-5: Modeling system for single inclusion migration in a thermal gradient field.

The modeling system is shown in Figure 2-5. A liquid-phase fluid inclusion enclosed in a closed surface Ω. We assume that the mass transfer within the inclusion can be described with a molecular diffusion process and that the thermal gradient within the inculsion is approxiamtely identail to the ambent gradient. Wthin Ω, we have:

$$\frac{\partial m}{\partial t} = D\nabla^2 m \qquad (2\text{-}1)$$

$$\frac{\partial T}{\partial x} = \alpha \qquad (2\text{-}2)$$

where m is the concentration of dissolved salt; D is the diffusion coefficient; T is the temperature; α is the thermal gradient; x is the coordination along the impose thermal gradeint; and t is the time.

On the inner surface Ω, mineral dissolution and precipitation takes place:

$$NaCl(s) \leftrightarrow NaCl(aq).$$

The mass balance on the surface can be described by:

$$R_d = k(K_d - m) \quad (2\text{-}3)$$

$$K_d(T,\ \kappa) = K_d^0 e^{\frac{\Delta H_r}{RT}\left(\frac{T}{T_0}-1\right)-\frac{2\gamma V_m \kappa}{RT}} \quad (2\text{-}4)$$

$$-D\vec{\nabla}m \cdot \vec{n} = R_d \quad (2\text{-}5)$$

where R_d is the mineral dissolution rate; K_d is the solubility of the mineral; k is the reaction rate constant; T_0 is the temperature at the center of the inclusion; K_d^0 is the mineral solubility at temperature T_0; ΔH_r the enthalpy of the mineral dissolution reaction; γ is the surface energy of the solution-salt interface; V_m is the molar volume of the salt; κ is the curvature of the surface; R is the gas constant; and $\vec{n}$ is the unit normal vector pointing inward (see Figure 2-5).

The evolution of inclusion surface can be described by the following kinematic equations (Wang and Merino, 1995):

$$\Omega(x, y, z, t) = 0 \quad (2\text{-}6)$$

$$\vec{\nabla}\Omega \cdot \vec{V} + \frac{\partial \Omega}{\partial t} = 0 \quad (2\text{-}7)$$

$$\vec{V} + V_0\vec{\imath} = -V_m R_d \vec{n} \quad (2\text{-}8)$$

$$\vec{n} = -\frac{\vec{\nabla}\Omega}{|\vec{\nabla}\Omega|} \quad (2\text{-}9)$$

$$\kappa = -\vec{\nabla} \cdot \vec{n} \quad (2\text{-}10)$$

where V_0 is the velocity of fluid inclusion migration; and $\vec{V}$ is the velocity of inclusion surface movement relative to the center of the inclusion. Equations (2-1) to (2-10) constitute a moving boundary problem for single fluid inclusion migration along a thermal gradient. This set of equations can be solved using a level-set method.

2.6 PRELIMINARY MODEL ANALYSIS

A first-order analysis has been conducted based on the model developed above. For a spherical liquid inclusion with a radius r, and assuming $k \to \infty$, the velocity of inclusion migration under a thermal gradient α can be estimated by:

$$V_0 \approx \frac{V_m D K_d^0 \Delta H_r \alpha}{R T_0^2} e^{-\frac{2\gamma V_m}{R T_0 r}} \quad . \qquad (2\text{-}11)$$

This simple equation can qualitatively explain the following key features experimentally observed:

- The model predicts a linear increase in migration evelocity with increasing thermal gradient α, as observed (Figure 2-4A).
- The model predicts that, as the size of the inclusion increases, the velocity of inclusion migration increases and then approaches a plateau (Figure 2-6). Also, as the temperature increases, the surface energy γ is expected to decrease (Ghanbaradeh et al., 2015) (Figure 2-7), thus shifting the plateau upward. Furthermore, as the size of the inclusion decreases, the migration velocity diminishes. All these predictions are qualitatively consistent with the observations (Figure 2-4B).
- Both terms D and K_d^0 in equation (2-11) expeonentailly increase with temperature. At elevated temperatures, the two terms are expected to take over the term T_0^2 in the denominator in the equation, leading to an overall exponential increase in migaration velocity with temperature, as shown in Figure 2-4C.
- Since the solubility of a mineral depends on the stress to which the mineral is subjected (Wang, 2016). A high mechanical loading results in a higher solubility of the mineral, therefore acelerating inclusion migration (Figure 2-4A).

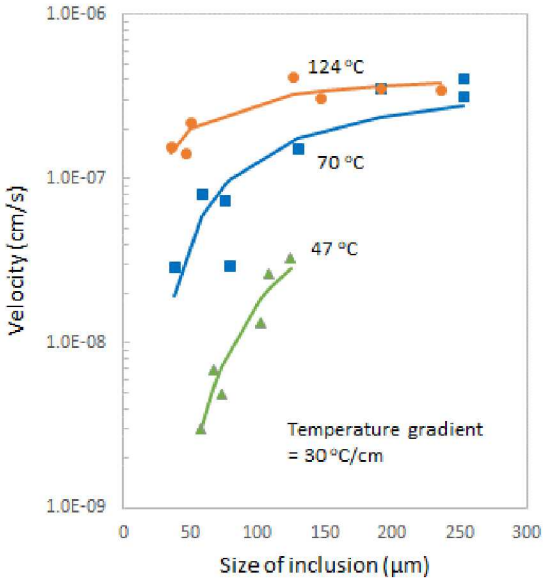

Figure 2-6. Fitting of equation (2-11) to the data shown in Figure 2-4B.

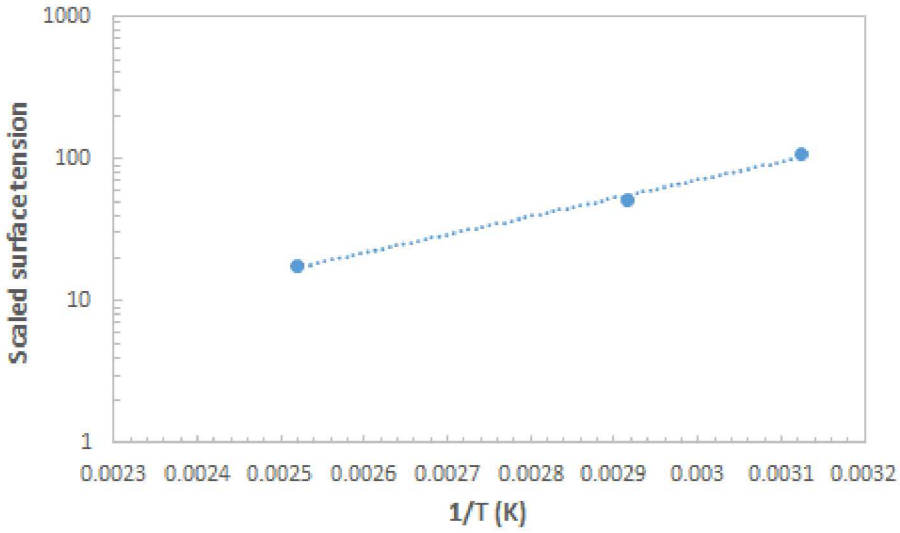

Figure 2-7. Temperature dependence of estimated surface tension of the interface between brine and solid.

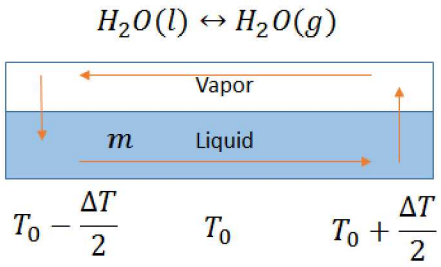

Figure 2-8: A simplified representation of a biphase fluid inclusion, in which a continuous vapor-liquid conversion takes place along a thermal gradient.

Simiarly, a preliminary analysis for biphase fluid inclusions has also been performed. For simplicity, a simple geometry of a fluid inclusion is assumed as shown in Figure 2-8. The mass continuity equations for both vapor and liquid as well as for the dissolved salt can be described by:

$$\rho_v(T) = \rho_v^0 e^{\frac{\Delta H_T^W}{RT}\left(\frac{T}{T_0}-1\right)} \quad (2\text{-}12)$$

$$A_v D_v \frac{\partial \rho_v}{\partial x} = A_l V_l \rho_w \quad (2\text{-}13)$$

$$-D\frac{\partial m}{\partial x} + mV_l = 0 \quad (2\text{-}14)$$

where ρ_v^0 is the vapor density at temperarture T_0; $\rho_v(T)$ is the vapor density at temperature T; ρ_w is the density of the liquid; ΔH_r^w is the enthalpy of liquid-vapor phase transition; A_v and A_l are the cross section areas of vapor and liquid respectively; D_v is the diffusion coefficient of vapor; and V_l is the local flow velocity of liquid. Assuming that the reaction rate for salt dissolution and precipitation $k \to \infty$, we obtain the bifurcation point in vapor/liquid volume ratio ($f = \frac{A_v}{A_l}$) for fluid inclusion migration:

$$f_c = \frac{D\Delta H_r \rho_w}{D_v \Delta H_r^w \rho_v^0(T_0)} \tag{2-15}$$

When $f > f_c$, the inclusion tends to move away from the heating surface, while for $f < f_c$, the inclusion tends to move upward the thermal gradient.

2.7 SUMMARY

Fluid inclusions can be found within mineral crystals or along grain boundaries in all types of sedimentary rocks. For a long-term performance assessment of a geologic repository, it is important to characterize the distribution, amount and interconnectivity of fluid inclusions in the host rock and to predict migration of these inclusions after waste emplacement. DECOVALEX Task F is designed to gain mechanistic understanding of possible physical processes involved in fluid inclusion migration in tight rocks such as rock salt or shale, with an ultimate goal to develop robust, predictive THMC modeling tools for a long-term performance assessment of a deep geologic repository in such media. The task will leverage the data provided by BGR, Germany. In fiscal year 2017, the work at SNL has focused on the model formulation of an individual fluid inclusion in rock salt. The model developed can qualitatively explain a number of key features of experimental observations. Specifically, the model can predict: (1) a linear increase in migration evelocity with increasing thermal gradient, (2) a nonlinear increase in migration velocity with inclusion size, (3) an overall aceleration in fluid migration with temperature, (4) the dependence of migration velocity on mechanical loadings. A preliminary analysis for biphase fluid inclusions has also been performed. A bifurcation point in vapor/liquid volume ratio for the direction of fluid migration is derived.

2.8 REFERENCES

Anthony, T. R. and Cline, H. E. (1971) Thermal migration of liquid droplets through solids, J. Applied Physics, 42, 3380-3387.

Anthony, T. R. and Cline, H. E. (1972) The thermomigration of biophase vapor-liquid droplets in solids, Acta Metallurgica, 20, 247-255.

Ghanbarzadeh, S., Hesse, M. A., Prodanović, M., Gardner, J. E. (2015) Deformation-assisted fluid percolation in rock salt, Science, 250, 1069-1072.

Hammer, Jörg, Pusch, Maximilian, Häger, Andreas, Scheeder, Georg, Shao, Hua, Paul, Benjamin, Ostertag-Henning, Christian, Mingerzahn, Gerhard, Schlömer, Stefan, Hesser, Jürgen (2013) Untersuchungen von Kohlenwasserstoffen im Erkundungsbergwerk Gorleben, BGR-Report, 2013.

Jenks, G. H. (1979) Effects of Temperature, Temperature Gradients, Stress, and Irradiation on Migration of Brine Inclusions in a Salt Repository, Oak Ridge National Laboratory, ORNL-5526.

Olander, D. R., Machiels, A. J., Balooch, M., Yagnik, S. K. (1982) Thermal gradient migration of brine inclusions in synthetic alkali halide single crystals, J. Applied Physics, 53, 669-681.

Roedder, E. (1984) The fluids in salt, American Mineralogist, 69, 413-439.

Wang, Y. (2016) On Subsurface fracture opening and closure, J. Petroleum Sci. Eng., 155, 46-53.

Wang, Y. and Merino, E. (1995) Origin of fibrosity and banding in agates from flood basalts, Am. J. Sci., 295, 49-77.

Yagnik, S. K. (1983) Interfacial stability of migration brine inclusions in alkali halide single crystals supporting a temperature gradient, J. Crystal Growth, 62, 612-626.

3. MODELLING GAS INJECTION EXPERIMENTS (ENGINEER)

3.1 INTRODUCTION

Rodwell et al. (1999) state "there are few problems in geoscience more complex than the quantitative prediction of gas migration fluxes through an argillaceous rock formation". To understand this statement, it is necessary to appreciate why clays and mudrocks differ from other clastic sedimentary rocks. Key factors in this respect include the sub-microscopic dimensions of the interparticle spaces, the very large specific surface of the mineral phases, strong physico-chemical interactions between water molecules and surfaces, very low permeability, generally low tensile strength, a deformable matrix, and a very pronounced coupling between the hydraulic and mechanical response of these materials. It is therefore necessary to consider these properties when defining the behavior of these materials in order to successfully represent flow in such systems.

With this in mind, the processes governing the movement of repository gases through engineered barriers and argillaceous host rocks can be split into two components, (i) molecular diffusion (governed by Fick's Law) and (ii) bulk advection. In the case of a repository for radioactive waste based on a generic KBS-3 concept, corrosion of metallic materials under anoxic conditions will lead to the formation of hydrogen. Radioactive decay of the waste and the radiolysis of water are additional source terms. If the rate of gas production exceeds the rate of gas diffusion within the pores of the barrier or host rock, a discrete gas phase will form (Weetjens and Sillen, 2006; Ortiz et al., 2002; Wikramaratna et al., 1993). Under these conditions, gas will continue to accumulate until its pressure becomes sufficiently large for it to enter the surrounding material.

In clays and mudrocks, four primary phenomenological models describing gas flow can be defined, Figure 3-1: (1) gas movement by diffusion and/or solution within interstitial fluids along prevailing hydraulic gradients; (2) gas flow in the original porosity of the fabric, commonly referred to as viscocapillary (or 2-phase) flow; (3) gas flow along localised dilatant pathways, which may or may not interact with the continuum stress field; and (4) gas fracturing of the rock similar to that performed during hydrocarbon stimulation exercises.

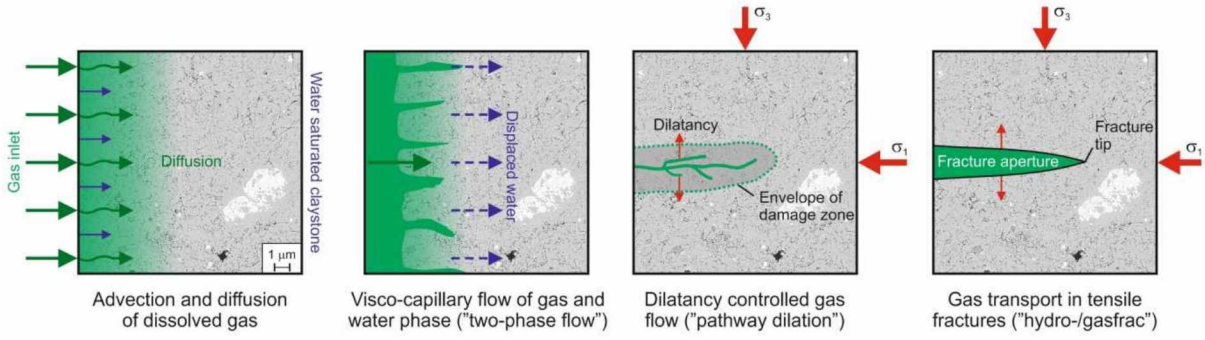

Figure 3-1: *Conceptual models of gas flow.*

There is now a growing body of evidence (Horseman et al., 1999, 2004; Harrington and Horseman, 1999; Angeli et al., 2009; Harrington et al., 2009) that in the case of plastic clays and in particular bentonite, classic concepts of porous medium two-phase flow are inappropriate and continuum approaches to modelling gas flow may be questionable, depending on the scale of the processes and resolution of the numerical model. However, the detail of the dilatant mechanisms controlling gas entry, flow and pathway sealing are unclear and the "memory" of such features within clay may impair barrier performance, in particular, acting as preferential flow paths for the movement of radionuclides.

As such, development of new and novel numerical representations for the quantitative treatment of gas in clay-based repository systems are therefore required, and are the primary focus of this Task. These will provide an invaluable tool with which to assess the impact of gas flow on repository layout and therefore design of any future facility. In addition, the same processes and mechanisms described in such models are of direct relevance to other clay-based engineering issues where immiscible gas flow is involved e.g. shale gas, hydrocarbon migration, carbon capture and storage and landfill design. The Task is split into a number of stages each building on the previous, representing an incremental increase in complexity. For each stage a specific experiment(s) will be presented and a series of constraints, variables and metrics stated in order to adequately define the scope of the Task.

Activity	Spring 2016	Autumn2 016	Spring 2017	Autumn 2017	Spring 2018	Autumn 2018	Spring 2019	Autumn 2019
Stage 0: code development								
Stage1 A & B: 1D flow (laboratory)								
Stage 2 A & B: Spherical flow (laboratory)								
Interim reporting								
Stage 3A: Gas flow in natural clay								
Stage 3B: Gas flow in pelletised bentonite								
Final Reporting								

3.2 NONLINEAR DYNAMICS OF GAS MIGRATION IN COMPACTED CLAY

In fiscal year 2017, the work at Sandia National Laboratories (SNL) has emphasized on the conceptual model development for gas migration in compacted clay materials. The model focuses on the nonlinear dynamic aspects of the process observed in experiments. As shown in Figure 3-2, gas migration in a water saturated compacted clay material exhibits rich nonlinear dynamic behaviours as the injection gas pressure varies: from a constant out flow to a periodic outflow and eventually to a chaotic behaviour. To test if the outflow variation is truly chaotic, we performed a time series analysis for one segment of outflow rate measurements (Figure 3-3). We first decompose the time series multiplicatively into three components: trend, periodic and stochastic components (Figure 3-3). It is interesting to note that the trend and periodic components account for most of the variability of the time series, indicating a possible existence of a deterministic internal structure in these dynamic data. We then calculated the embedded dimension using the false nearest neighbor method for the system (Strogatz, 2001). It is found the embedded dimension of the system ranges from 3 to 4 (Figure 3-4). Furthermore, we plotted the time series in an embedded space (Figure 3-5). It is shown that in the embedded space the outflow seems to possess an internal structure, i.e., not completely random (white noise), indicating a deterministic chaotic behavior.

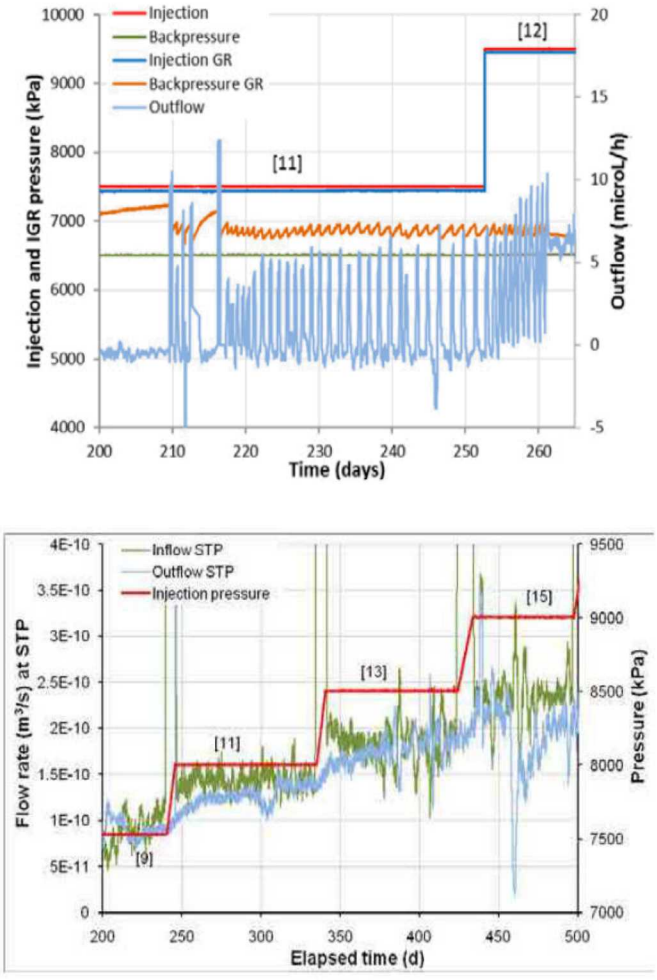

Figure 3-2: Nonlinear behaviors of gas migration in water saturated compacted clay materials (Cuss et al., 2012).

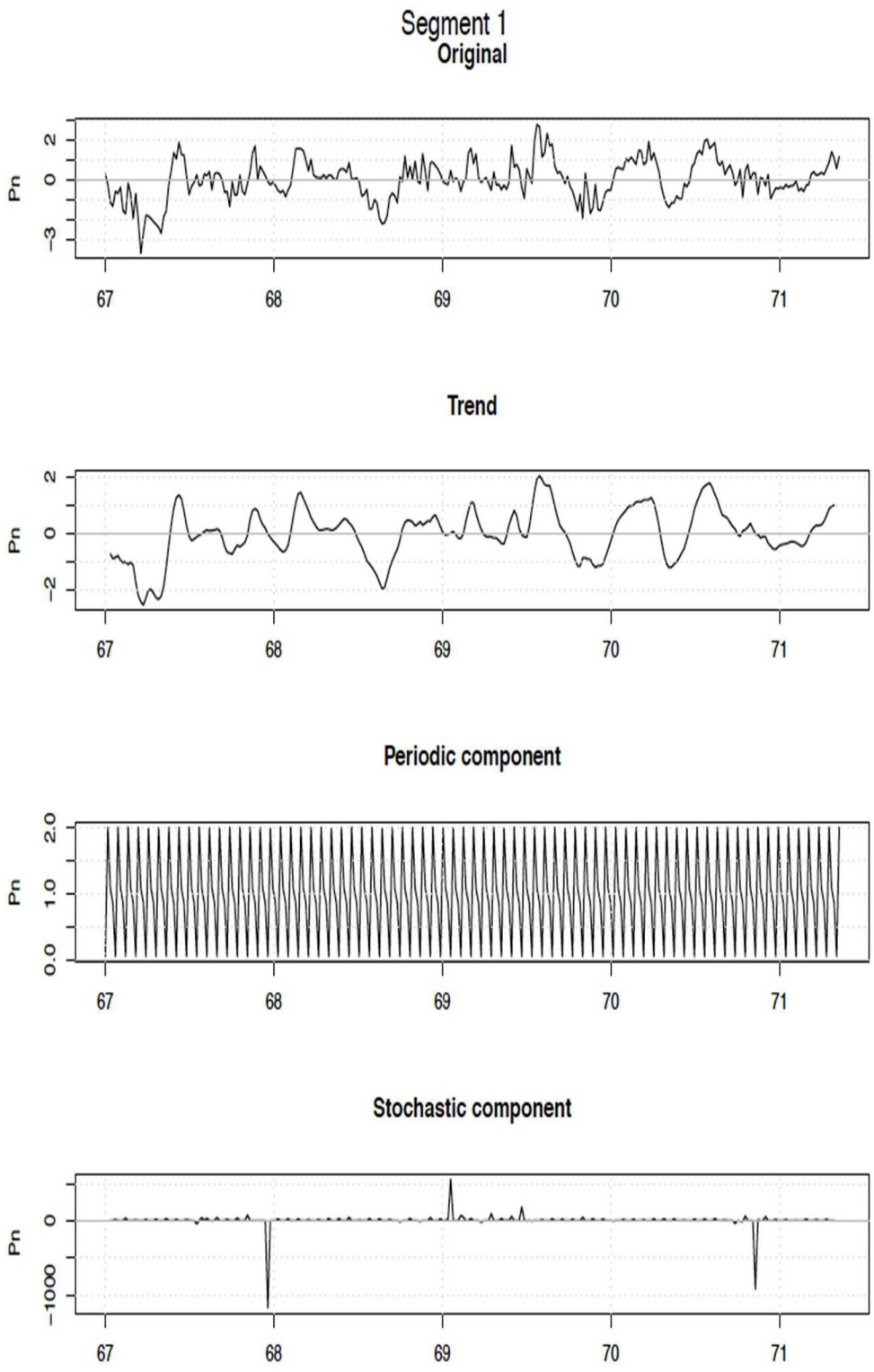

Figure 3-3: Outflow rate time series and multiplicative decomposition of the data.

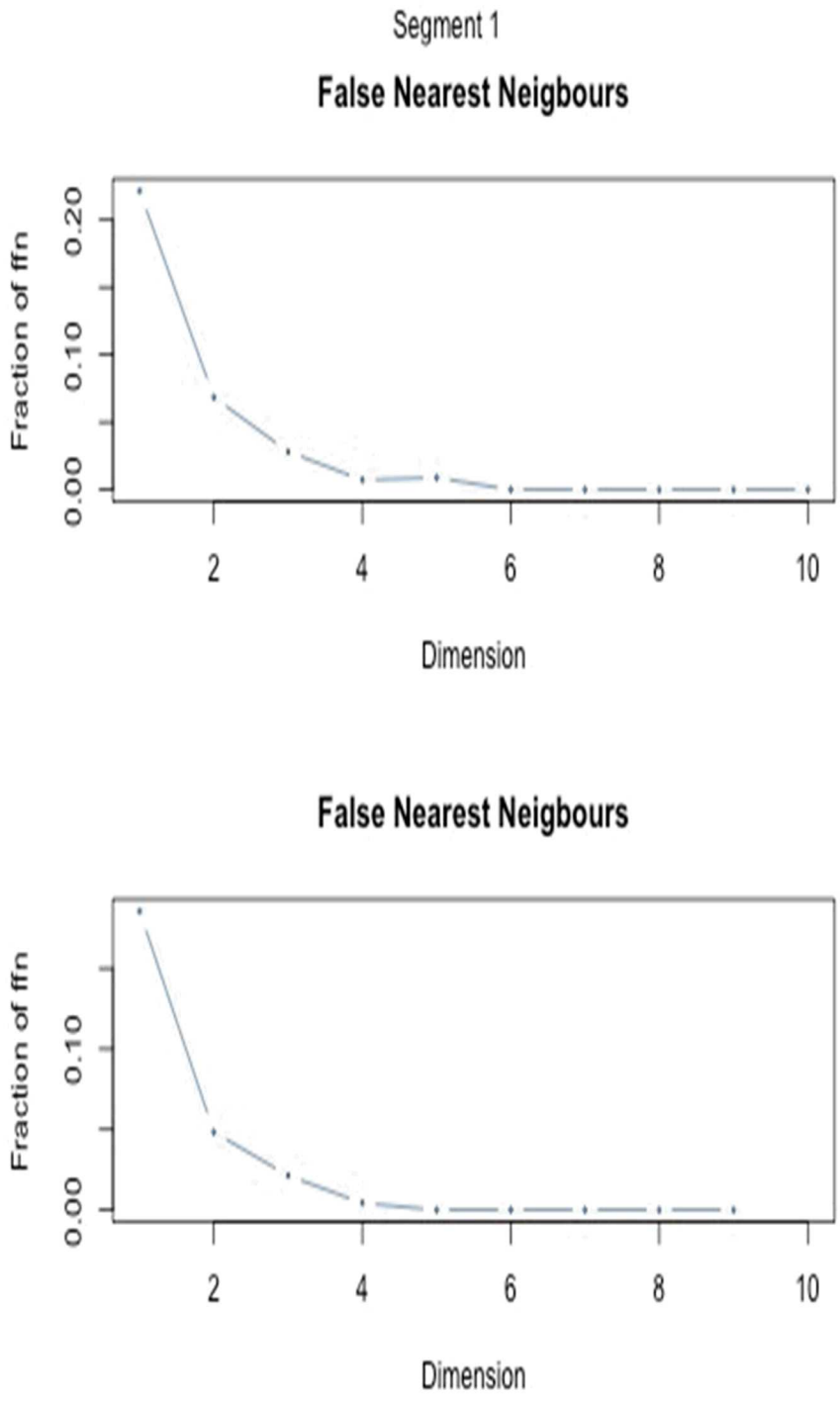

Figure 3-4: Embedded dimension calculated using the false nearest neighbor methods.

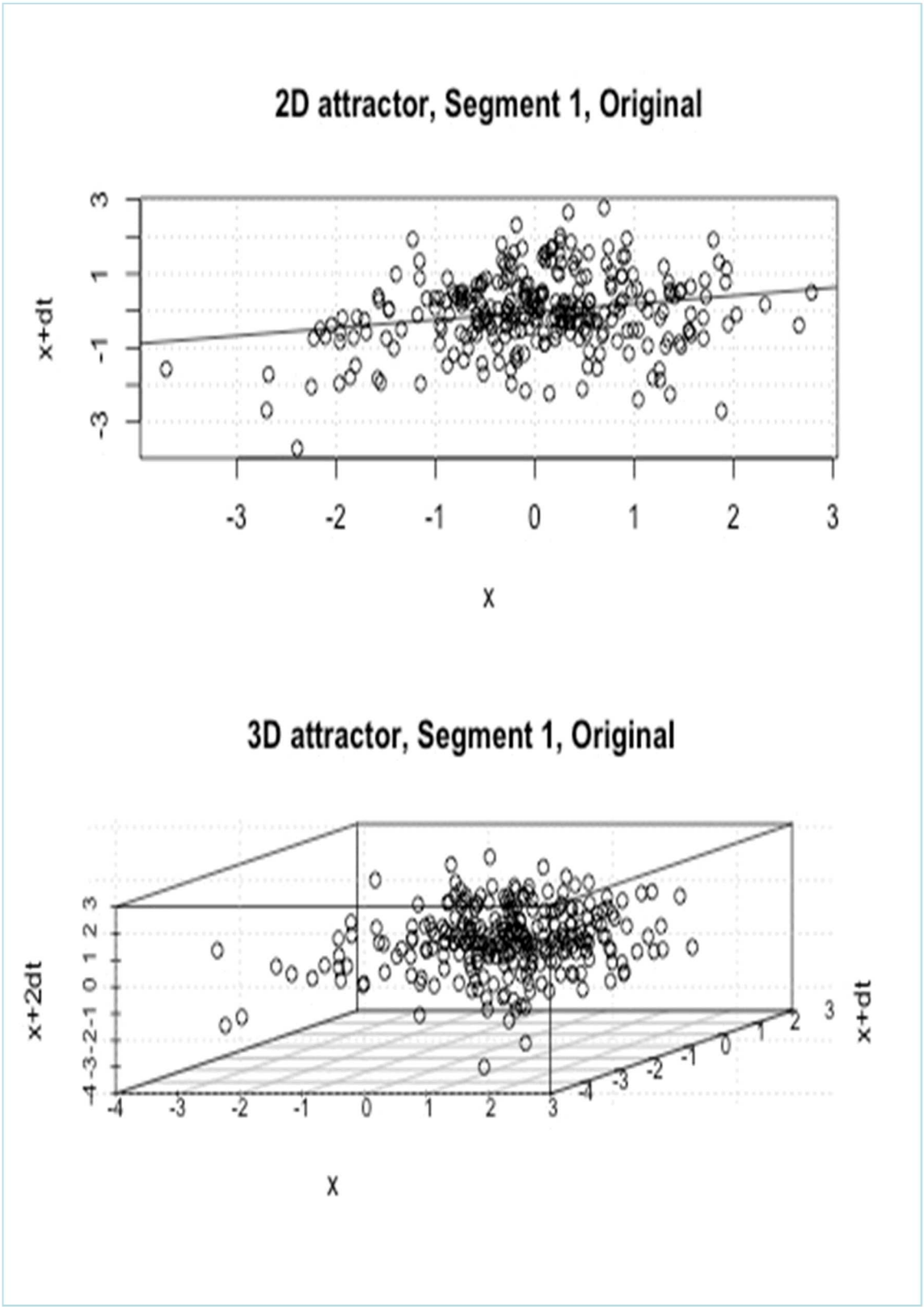

Figure 3-5: 2D and 3D pseudo-phase attractors in the embedded space.

To explain these dynamic behaviors, we have developed a chaotic model based on the concept of delay logistic model (Strogatz, 2001; Bani-Yaghoub, 2017). For illustration, we focus on single gas bubble movement in a compacted clay material under a gas pressure gradient (Figure 3-6). The underlying assumption is that, given a low permeability of the material, the dominant mechanism for gas migration is first to form a bubble nucleation and then to push the bubble through the clay matrix through matrix dilation and fracturing. In the wake of bubble movement, matrix compression and fracture healing may also take place. With this assumption, the evolution of mass and pressure within a bubble of a volume V can simply expressed by:

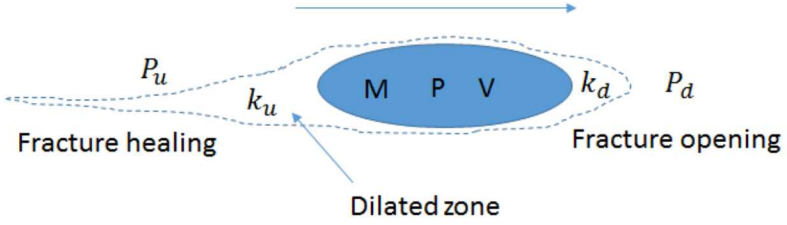

Figure 3-6: Conceptual model for gas bubble movement in a compact clay material under a pressure gradient.

$$\frac{dM}{dt} = k_u(P_u - P) - k_d(P - P_d) \quad (3\text{-}1)$$

where M is the gas mass in the bubble; P is the gas pressure in the bubble; P_u and P_d are the gas pressures in the upstream and the downstream of the bubble movement respectively; k_u and k_d are the permeability of the matrix in the upstream and the downstream of the bubble movement respectively; and t is the time. Considering a possible effect of dilation, fracturing and fracture healing on matrix permeability, we assume that k_u and k_d are proportional to the gas pressure P:

$$k_u = k_u^0 P \quad (3\text{-}2)$$

$$k_d = k_d^0 P \quad (3\text{-}3)$$

where k_u^0 and k_d^0 are constant. With the ideal gas law $M = \frac{PV}{RT}$, where R is the gas constant and T is the temperature, the equation (3-1) can be cast into:

$$\frac{dP}{dt} = \lambda_1 P\left(1 - \frac{P}{K}\right) \quad (3\text{-}4)$$

Equation (3-4) is a continuous logistic equation, with

$$\lambda_1 = \frac{(k_u^0 P_u + k_d^0 P_d)RT}{V} \quad (3\text{-}5)$$

$$\lambda_2 = \frac{(k_u^0 + k_d^0)RT}{V} \quad (3\text{-}6)$$

$$K = \frac{\lambda_1}{\lambda_2} \, . \quad (3\text{-}7)$$

As discussed above, clay matrix may have a memory effect on deformation and fracturing, which implies that the permeabilities k_u and k_d depends not only on the current pressure value but also the recent history of the pressure, which can be captured by the following delay logistic equation:

$$\frac{dP}{dt} = \lambda_1 \left(1 - \frac{P}{K}\right) \int_{-\infty}^{t} G(t-s)p(s)ds \qquad (3\text{-}8)$$

where $G(t)$ is a kernel function characterizing the influence of the pressure at a previous step on the permeability at the current time step. A commonly chosen kernel function is an exponential function characterizing an exponential decay of the influence as the time interval increases:

$$\frac{dP}{dt} = \lambda_1 \left(1 - \frac{P}{K}\right) \int_{-\infty}^{t} \alpha e^{-\alpha(t-s)} p(s)ds. \qquad (3\text{-}9)$$

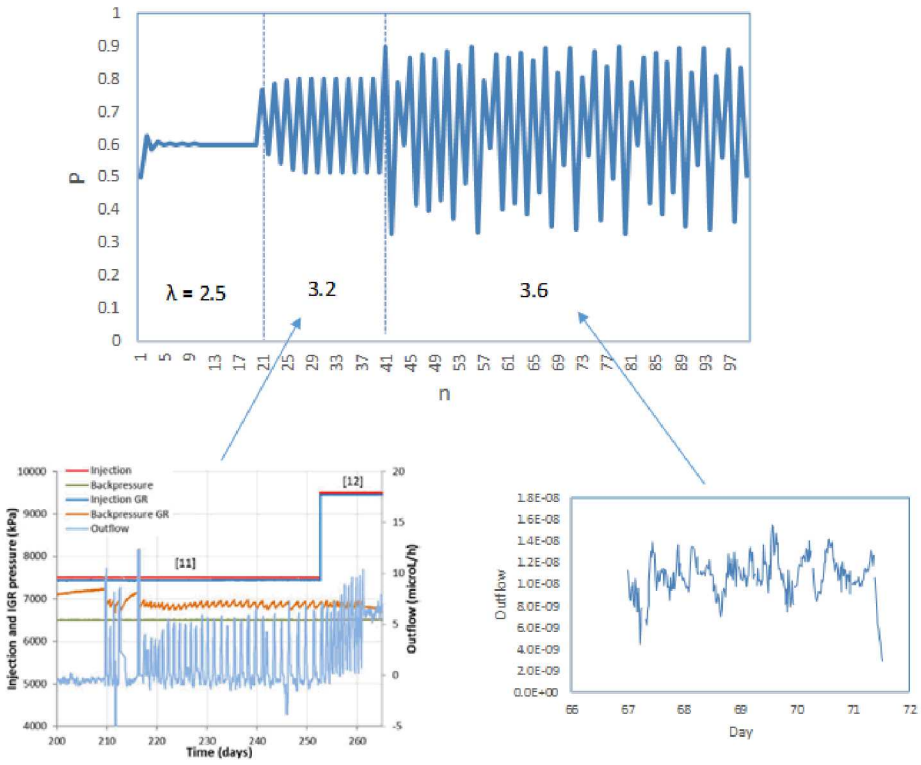

Figure 3-5: Explanation of gas migration dynamics from a chaotic point of view. Experimental measurements are from Cuss et al. (2012).

For an illustration of the concept of bifurcation and chaos for gas migration, let's assume the gas movement is more or less stepwise. Equation (3-4) can then be reduced to a logistic map:

$$p_{n+1} = \lambda p_n (1 - p_n) \qquad (3\text{-}10)$$

with

$$\lambda = 1 + \lambda_1 \Delta t \qquad (3\text{-}11)$$

where is a scaled gas pressure inside the bubble. It is known that Equation (3-10) can exhibit rich dynamic behaviors (Strogatz, 2001) as shown in Figure 3-5.

3.3 SUMMARY

Bentonite has been proposed as a buffer material for a deep geologic repository. Understanding gas migration in compacted clay materials is important for a performance assessment of an engineered barrier system of a repository system. Existing data demonstrate the complexity of gas migration in such low-permeability materials. Through a simple model analysis, we here show that this complexity can probably be explained with a bifurcation and chaos concept. The dynamic behavior of the system has been shown closely related to clay matrix dilation, fracturing and fracture healing as induced by gas bubble movement. The concept proposed here provide a new perspective for modeling gas migration in low-permeability materials.

3.4 REFERENCES

Angeli, M., Soldal, M., Skurtveit, E. and Aker, E. (2009) Experimental percolation of supercritical CO_2 through a caprock. Energy Procedia,1, 3351-3358.

Bani-Yaghoub, M. (2017) Analysis and applications of delay differential equations in biology and medicine, arXiv:1701.04173v1.

Cuss, R. J., Harington, J. F., and Noy, D. J. (2012) Final Report of FORGE WP4.1.1: Stress-Path Permeameter Experiment Conducted on Callovo-Oxfordian Claystone, British Geological Survey, Minerals and Waste Programme Commissioned CR/12/140.

Harrington, J.F. and Horseman, S.T. (1999). Gas transport properties of clays and mudrocks. In: Muds And Mudstones: Physical And Fluid Flow Properties (eds A.C.Aplin, A.J. Fleet, and J.H.S. Macquaker). Geological Society of London, Special Publication No. 158, 107-124.

Horseman, S.T., Harrington, J.F. and Sellin, P. (1999). Gas migration in clay barriers. Engineering Geology, Vol. 54, 139-149.

Horseman, S.T., Harrington, J.F. and Sellin, P. (2004) Water and gas flow in Mx80 bentonite buffer clay. In: Symposium on the Scientific Basis for Nuclear Waste Management XXVII (Kalmar), Materials Research Society, Vol. 807. 715-720.

Harrington, J.F., Noy, D.J., Horseman, S.T., Birchall, J.D. and Chadwick, R.A. (2009) Laboratory study of gas and water flow in the Nordland Shale, Sleipner, North Sea. Pp. 521-543 in: Carbon Dioxide Sequestration in Geological Media State of the Science (M. Grobe, J.C. Pashin and R.L. Dodge, editors). AAPG Studies in Geology, 59. American Association of Petroleum Geologists, Tulsa, Oklahoma, USA.

Ortiz, L., Volckaert, G. and Mallants, D. (2002) Gas generation and migration in Boom Clay, a potential host rock formation for nuclear waste storage. Engineering Geology, 64, 287-296.

Rodwell W R, Harris A W, Horseman S T, Lalieux P, Müller M, Ortiz Amaya L, Pruess K, 1999. Gas migration and two-phase flow through engineered and geological barriers for a deep repository for radioactive waste. EC/NEA Status Report EUR 19122EN, European Union, Luxembourg.

Strogatz, S. H. (2001) Nonlinear Dynamics and Chaos: With Applications to Physics, Biology, Chemistry, and Engineering, Westview.

Weetjens, E. and Sillen, X. (2006) Gas Generation and Migration in the Near Field of a Supercontainer-Based Disposal System for Vitrified High-Level Radioactive Waste. Proceedings of the 11th International High-Level Radioactive Waste Management Conferance (IHLRWM), Las Vegas, Nevada, USA.

Wikramaratna, R.S., Goodfield, M., Rodwell, W.R, Nash, P.J. and Agg, P.J. (1993) A Preliminary Assessment of Gas Migration from the Copper/Steel Canister. SKB Technical report TR93-31. Swedish Nuclear Fuel and Waste Management Company (SKB), Stockholm, Sweden.

4. DEVELOPMENT AND VALIDATION OF A FRACTURE MODEL FOR THE GRANITE ROCKS AT MIZUNAMI UNDERGROUND RESEARCH LABORATORY, JAPAN

4.1 INTRODUCTION

The Mizunami Underground Research Laboratory (MIU) is located in the Tono area (Central Japan). Its main purpose is to provide a scientific basis for the research and development of technologies needed for deep geological disposal of radioactive waste in fractured crystalline rocks. The site hydrology is described in Iwatsuki et al. (2005) and Iwatsuki et al. (2015). A large amount of fracture data was collected in the Tono area. The fracture data analysis and development of the fracture models at the different scales is an ongoing effort. Bruines et al. (2014) described the development of the discrete fracture network models for 2 scales – local (9km x 9km) and site-scale (2km x 2km). Both models extend from the surface to the depth of 2 km and are based on the data from MIU Project Phase I and II investigations. The fractured rocks are composed of Toki granite. The upper portion of the Toki granite, known as the Upper Highly Fractured Domain (UHFD), is better characterized. Significantly less data is available for the lower portion, known as Lower Sparsely Fractured Domain (LSFD). Some data for LSFD can be found in JAEA report (Ando et al., 2012) for boreholes DH-2, DH-15 and MIZ-1. The current work at the MIU focuses on the experiments in the research tunnel (500 m depth). The modeling domain considered in this study is within the LSFD and includes the area surrounding the research tunnel. The model occupies a very small volume of the site-scale model considered in Bruines et al. (2014).

The data used to develop the fracture model in this report are primarily based on the Research tunnel fracture traces and fracture observations in borehole 12MI33. A portion of borehole MIZ-1 is within the modeling domain. The other boreholes are outside the modeling domain. These data were shared with the participants of DEvelopment of COupled models and their VALidation against EXperiments (DECOVALEX) project.

4.2 APPROACH TO DEVELOPING DISCRETE FRACTURE NETWORK

The discrete fracture network (DFN) model was developed for the area surrounding the MIU Research tunnel at 500 m depth using FRACMAN (Golder Associates, Inc., 2017). This model will be a major tool for simulating hydrogeologic and geochemical conditions in the various experiments being conducted in the Research tunnel. The observed inflow into the tunnel during the excavation was used to validate the model.

The modeling domain is 100x150x100m with the main experimental part of the tunnel, Closure Test Drift (CTD), located approximately in the center. Figure 4-1 shows the modeling domain, the research tunnel (CTD and Inclined Drift), the horizontal monitoring borehole 12MI33 (with 6 test intervals), and the vertical exploratory borehole MIZ-1 (only 2 test intervals are inside the modeling domain).

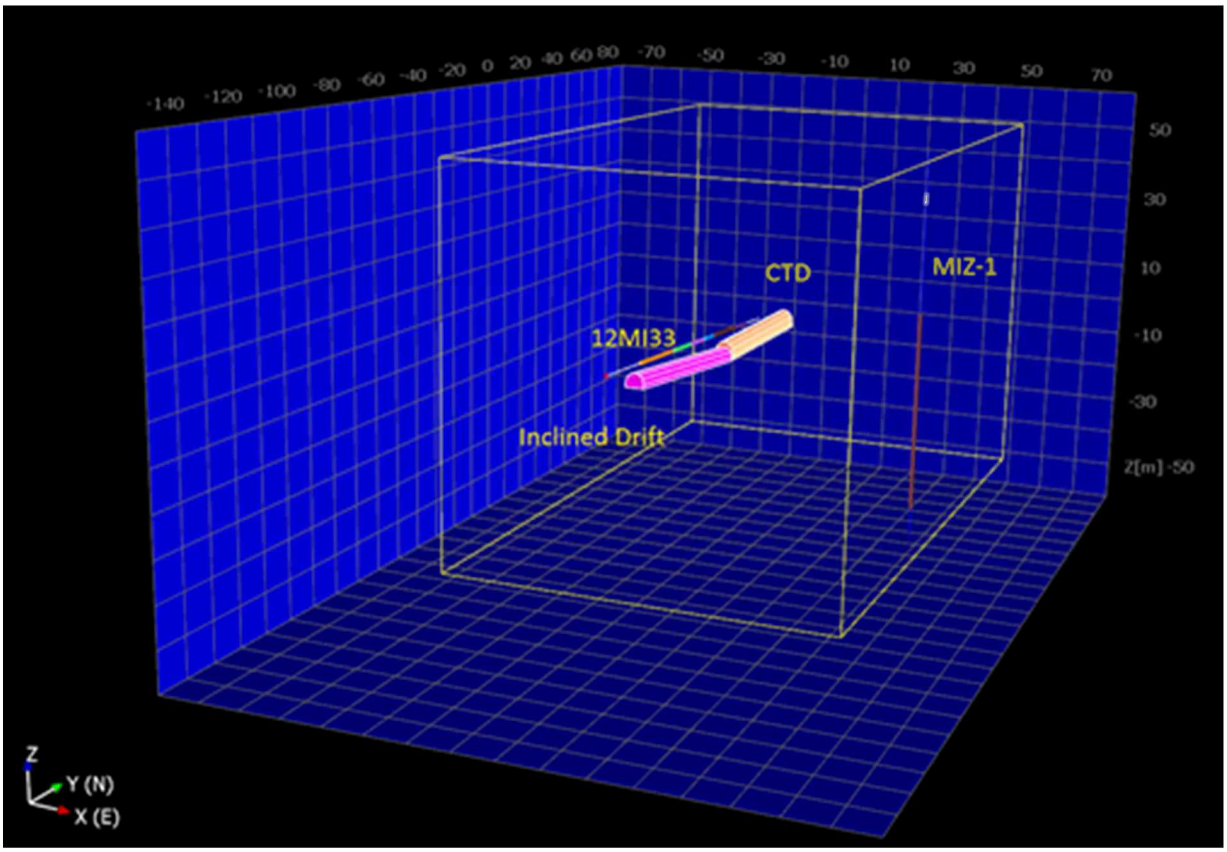

Figure 4-1: Modeling domain and location of research tunnel and boreholes.

The following data were used in the fracture analysis:

- Fracture traces on the walls of CTD, Inclined Drift, and Access Drift (Figure 4-2). Note that Access drift fracture data were used in the analysis even though this drift is outside the modeling domain.
- Fractures observed in borehole 12MI33.
- Packer test data in 6 test intervals of 12MI33.
- Measured inflow into the research drift.

Two thousand and twenty-three fractures were observed on the wall of the research tunnel. It was assumed that the fractures that did not exhibit any flow discharge are either closed fractures or small fractures not connected to the fracture network. There are 146 fractures (7.2%) with the observed flow discharge. They are characterized in the original data set based on the flow range as “flow” (F) fractures (>1L/min), “drop” (D) fractures (>0.1L/min), and “wet” (W) (<0.1L/min) fractures.

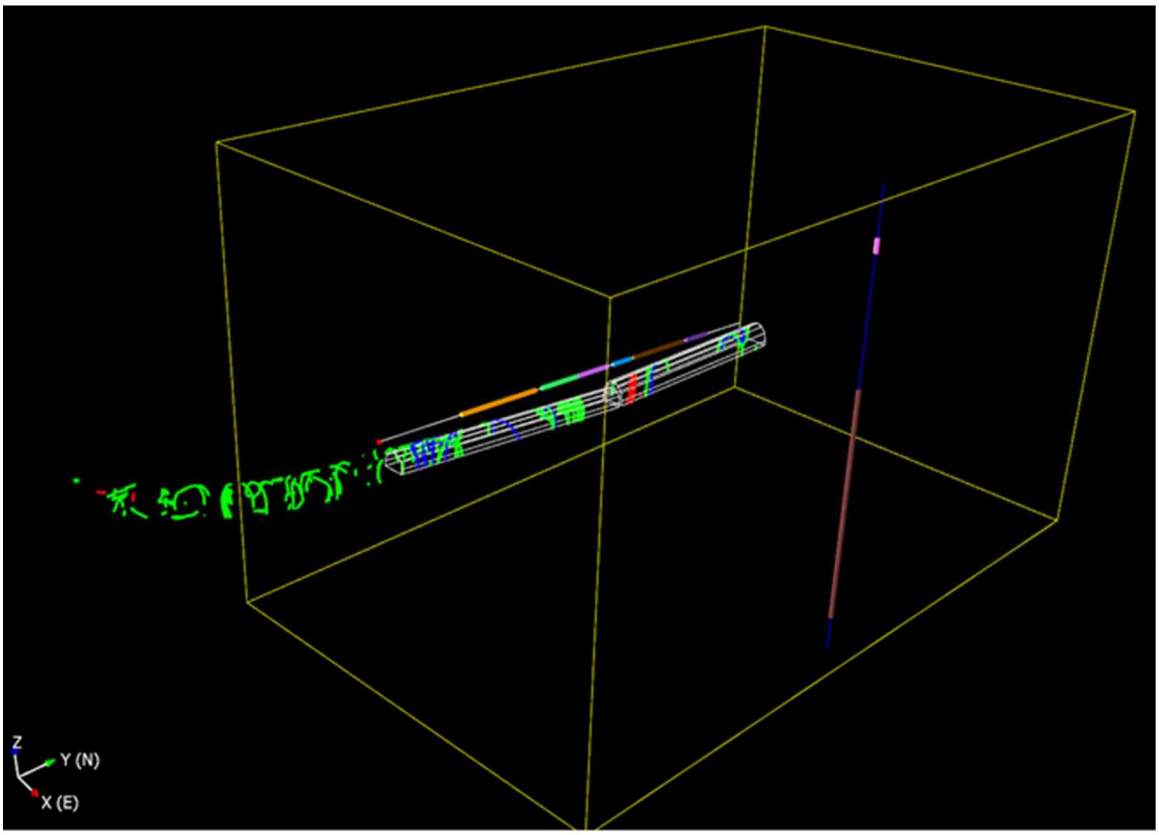

Note: F-fractures are shown in blue, D-fractures are shown in green, and W-fractures are shown in red color.

Figure 4-2: Traces of the fractures on the Research tunnel walls included in the analysis.

The fracture size was derived from the trace length analysis. It was assumed that the fractures with different flow discharges may have different sizes. Consequently, the analysis was conducted separately for F-, D-, and W- fractures. The trace length distributions of all sets are best described with the lognormal distribution (Table 4-1). The distributions of W- and D- fractures are very similar and were combined in one. The F-fractures with greater flow rates are also the ones with the larger size.

Table 4-1: Equivalent fracture radius distribution parameters.

Fracture Set	Distribution Type	Mean Radius (m)	Standard Deviation (m)
D- and W-Fractures	Lognormal	1.42	1.29
F-Fractures	Lognormal	3.88	2.15

The initial evaluation of fracture transmissivity was based on the observed range of flow through the different types of fracture. The analytical solution for the unit inflow (Q) into a circular tunnel with radius r located at depth h (Butscher, 2012) is:

$$Q = \frac{2\pi k(A+H)}{\ln(\frac{h}{r})+\sqrt{\frac{h^2}{r^2}-1}} \quad (4\text{-}1)$$

where k is the hydraulic conductivity, H is hydraulic head, and A is defined as:

$$A = h(1-\alpha^2)/(1+\alpha^2) \text{ and } = \frac{1}{r}(h-\sqrt{h^2-r^2} \quad (4\text{-}2)$$

The inflow through the fracture Q_{fr} [m^3/s] with aperture b [m] perpendicular to the tunnel is:

$$Q_{fr} = Q \cdot b = \frac{2\pi T(A+H)}{\ln(\frac{h}{r})+\sqrt{\frac{h^2}{r^2}-1}} \quad (4\text{-}3)$$

where $T = k \cdot b$ is fracture transmissivity of the single vertical fracture [m^2/s].

The lower (or upper) fracture transmissivity limit T was calculated from Eq. 4-3 assuming r = 2.5 m, h = 500m, and H = 110m. The transmissivity of F- fractures (Q_{fr} > 1.0 L/min) is > 2.6*10^{-8} m^2/s, transmissivity of D- fractures (Q_{fr} > 0.1 L/min) is > 2.6*10^{-9} m^2/s, and the transmissivity of W- fractures (Q_{fr}< 0.1 L/min) is < 2.6*10^{-9} m^2/s. The observed inflows into CTD and Inclined Drift were used to adjust these limits until the good match was obtained (Table 4-2). The corresponding transmissivity values are: 6.0*10^{-8} m^2/s (F-fractures), 6.0*10^{-9} m^2/s (D- fractures), and 2.6*10^{-9} m^2/s (W- fractures). Assuming water density of 998 kg/m^3 and water viscosity of 0.001 N s/m^2 the fracture permeability values are: 1.5x10^{-10} m^2 (F-fractures), 3.2x10^{-11} m^2 (D-fractures) and 1.8x10^{-11} m^2 (W-fractures).

Table 4-2: Comparison of measured and calculated inflow into the Research tunnel.

Research Tunnel Segment	Measured Tunnel Inflow (L/min)	Number of Fractures			Calculated Inflow (L/min)			
		F	D	W	F	D	W	Total
CTD	13	4	15	3	9.2	3.45	0.3	12.95
Inclined Drift	43	14	42	N/A	32.2	9.66	0	41.86

The calculated transmissivity (permeability) represents the average values. There is no enough data to develop probability distributions for these parameters. Very few data are available on fracture aperture. This analysis assumed correlations between the lognormally distributed fracture equivalent radius (R) and fracture permeability (k) and aperture (b) in the following form:

$$k = \gamma_1 \cdot R^{\omega} \quad (4\text{-}4)$$

$$b = \gamma_2 \cdot R \quad (4\text{-}5)$$

where γ_1, γ_2, and ω are coefficients.

Equation 4-3 was used to calculate the inflow through each of 146 fractures generated in the Research Tunnel using the lognormal fracture radius distributions (Table 4-1). The total calculated inflow was compared to the observed inflow. A good match (113 L/ versus 104 L/min) was obtained with the following coefficient values:

- $\gamma_1 = 1.55 \times 10^{-12}$
- $\gamma_2 = 1.16 \times 10^{-5}$
- $\omega = 2.3$

The transmissivity estimates were corroborated by comparing the packer test results with the transmissivity of fractures generated in borehole 12MI33. Borehole 12MI33 is a horizontal borehole that is parallel to the Research tunnel (Figure 4-1). The packer tests were conducted in 6 test intervals. The test intervals also serve as the monitoring points (for observation of temporal variations in pressure and geochemistry in vicinity of the Research tunnel). Two hundred and ninety-seven fractures were recorded in the borehole. The fractures were classified as "crack", "hair crack", "discontinuity crack", and "mineral vein". The fractures described as cracks that had recorded aperture values were assumed to be permeable fractures, such as F-, D-, and W-fractures observed in the Research tunnel.

The fractures generated in the borehole are shown in Figure 4-3 along with the Research tunnel fractures. Figure 4-3 also shows the transmissivity of the test intervals obtained in the packer tests. The high transmissivity intervals 1, 2' and 6 coincide with the zones in which fractures generated in both, Research tunnel and borehole, are present. Intervals 2 and 3 intersect a few fractures and their transmissivity is lower. Intervals 4 and 5 do not intersect any of generated fractures and their transmissivity is significantly lower. The locations of 17 fractures generated in borehole 12MI33 are consistent with the locations of fractures in the Research tunnel.

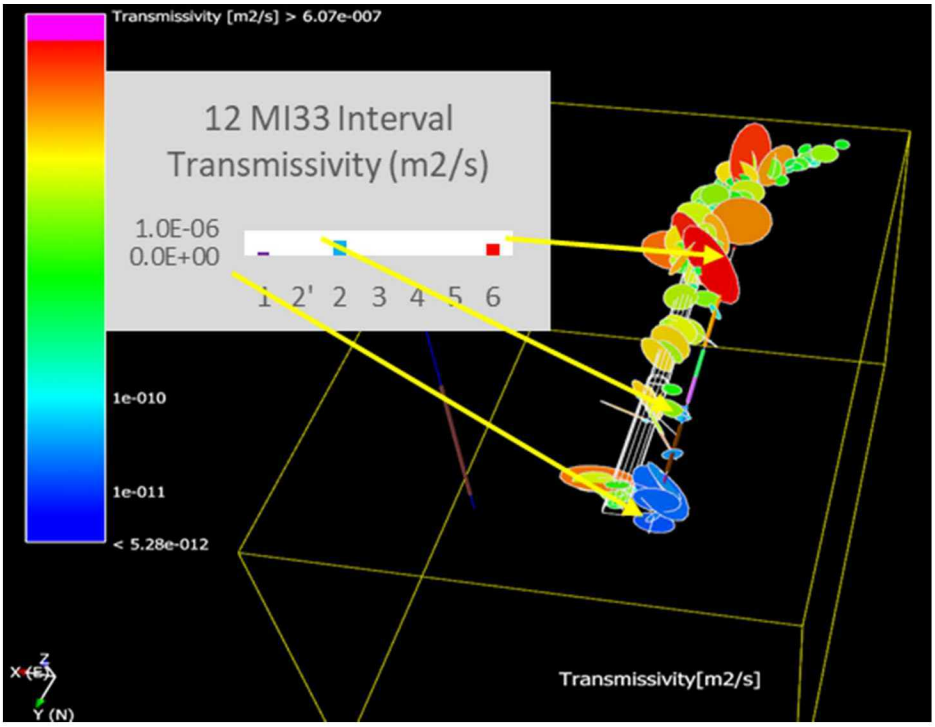

Figure 4-3: Transmissivity of fractures in the Research tunnel and borehole 12MI33.

The transmissivities of the fractures generated in borehole 12MI33 were compared to the transmissivity of the test intervals from the packer tests in this borehole. The total transmissivity of the fractures generated in the borehole ($7.6x10^{-7}$ m^2/s) is close to the total transmissivity of the test intervals ($9.9x10^{-7}$ m^2/s). Consequently, the fracture properties derived from the Research tunnel fracture trace analysis are consistent with the packer test data in borehole 12MI33.

It can be assumed that the fractures located outside the Research tunnel and borehole 12MI33 have the same parameter distributions as the fractures in the Research tunnel and borehole 12MI33. However, generation of these fractures requires additional parameters, such as the number of fracture sets, orientation distribution of each set, and fracture intensity in each set.

The number of fracture sets and their orientation was obtained from the analysis of the fractures generated from the tunnel traces. Figure 4 shows the fracture set assignment results for the Research tunnel fractures.

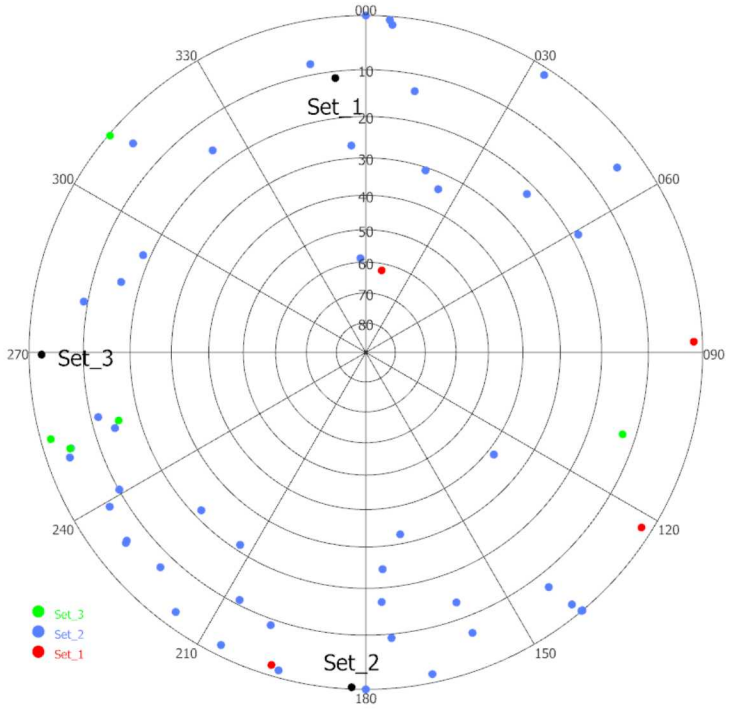

Figure 4-4: Fracture set assignment results for the Research tunnel fractures.

Three fracture sets were unidentified. The unilateral Fisher's distribution was found to be the best fit for all sets. However, set 3 in Figure 4-4 was removed from the analysis. This set contains fractures in the Access Drift. The Access drift is located outside the modeling domain and is affected by the nearby Main Shaft fault.

The properties of the two fractures sets incorporated in the model are provided in Table 4-3. Note that orientation is given in the local coordinate system. The actual coordinate system was rotated 10.20 clockwise in the x-y plane to align the tunnel with the y axis.

Table 4-3: Fracture Orientation Distributions.

Fracture Set	Trend (^{0})	Plunge (^{0})	Fisher Dispersion k	Volumetric Intensity P_{32} (1/m)
Set 1	208	8	7	0.22
Set 2	303	1.3	3.6	0.086

To evaluate volumetric intensity P_{32} of each fracture set the following approach was used. The stochastic fractures were generated using Fisher distributions (Table 4-3), fracture radius distributions (Table 4-1), fracture permeability (Eq. 4-4), and fracture aperture (Eq. 4-5). The P_{32} values were iteratively redefined until the linear intensity (P_{10}) values in two arbitrary placed imaginary horizontal boreholes matched P_{10} of fractures observed in the Research tunnel and borehole 12MI33. The calculated P_{32} values are provided in Table 4-3.

Figure 4-5 shows one realization of the DFN generated with the properties defined in Table 4-3. The DFN also contains fractures generated in the Research tunnel and borehole 12MI33. Figures 4-6 and 4-7 show the sampled distribution of fracture permeability and aperture for this realization.

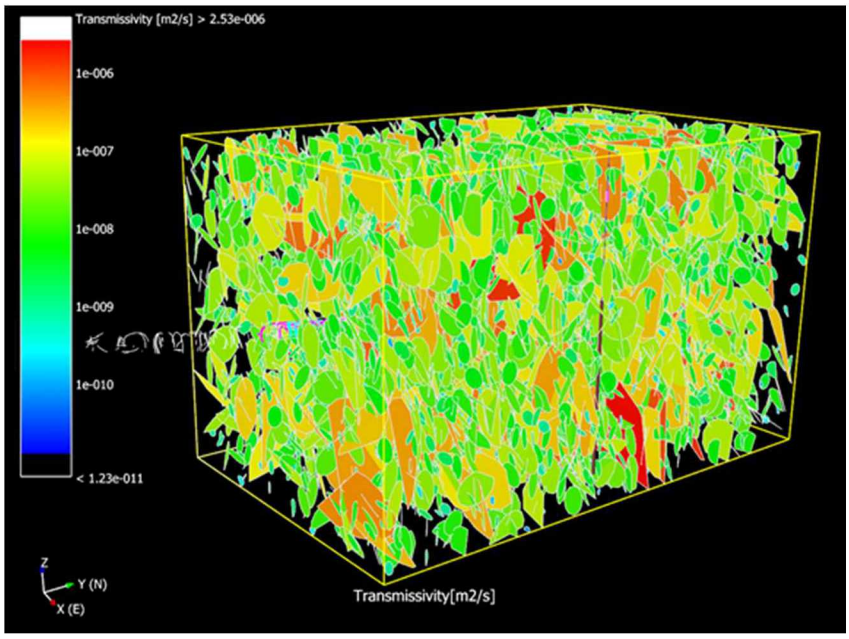

Figure 4-5: One realization of discrete fracture network.

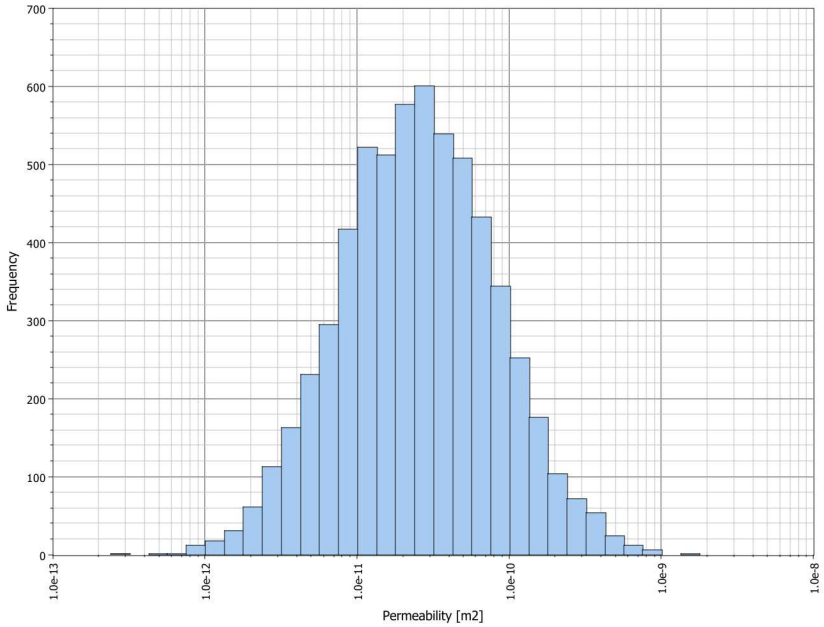

Figure 4-6: Sampled fracture permeability.

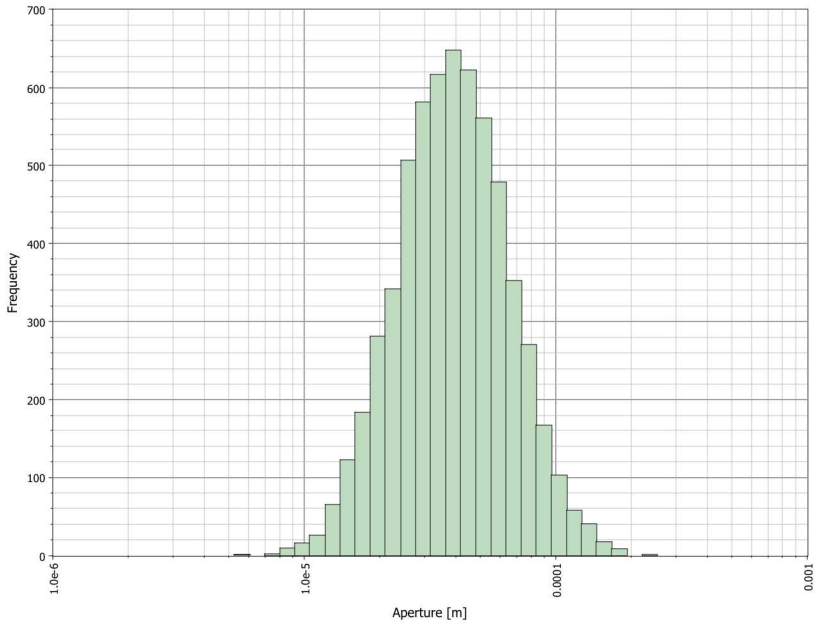

Figure 4-7: Sampled fracture aperture.

For flow and transport simulations, the DFN was upscaled to an equivalent continuum model with the uniform grid cell size of 1x1x1 m. The effective *x*, *y*, and *z* permeabilities and effective porosity were calculated for each grid cell containing fractures using Oda's method in FRACMAN. The permeability and porosity of the grid cells without fractures were defined in accordance with the matrix permeability and

porosity. Figure 4-8 shows vertical slice of the effective permeability in *z* direction for the DFN realization shown in Figure 4-5. Table 4-4 summarizes the mean properties of the grid cells in the modeling domain. There is noticeable anisotropy in permeability in *x*. *y*, and *z* directions

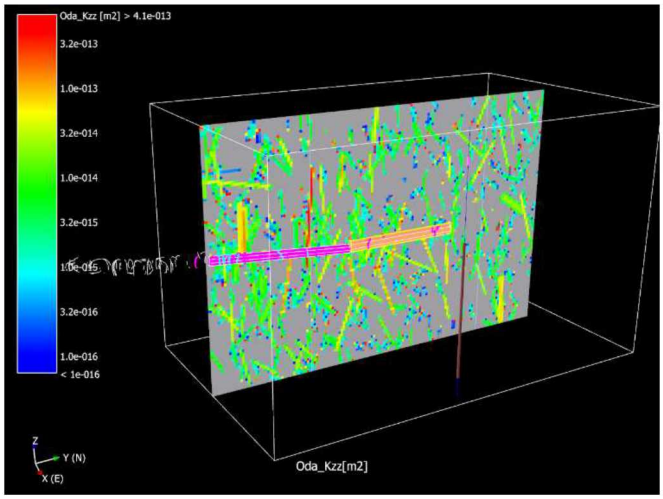

Figure 4-8: Vertical slice of effective permeability in z direction for DFN realization show in Figure 4-5.

Table 4-4: Effective Continuum Model Mean Grid Cell Properties.

Parameter	Notation	Mean Value
Permeability (m^2)	K_{xx}	3.50E-15
	K_{yy}	1.84E-15
	K_{zz}	4.15E-15
Fracture porosity	€	2.1E-05

4.3 MODEL VALIDATION

The developed effective continuum model was used to simulate the inflow into the Inclined drift and CTD during the tunnel excavation. The tunnel excavation was modeled by removing material with 1 m increments for a total of 103 m. The flow simulations were conducted with PFLOTRAN (Hammond et al., 2014), an open source, state-of-the-art massively parallel subsurface flow and reactive transport code. The details of flow simulations are presented in a companion paper by Hadgu et al. (2018).

Figure 4-9 compares the calculated and observed inflows. A very good agreement is obtained with the effective continuum model. Also shown in this figure is the simulation in which a homogeneous model was

with permeability of $1x10^{-15}$ m^2 was used. The homogeneous model is not capable of reproducing the observed values as well as the observed trend.

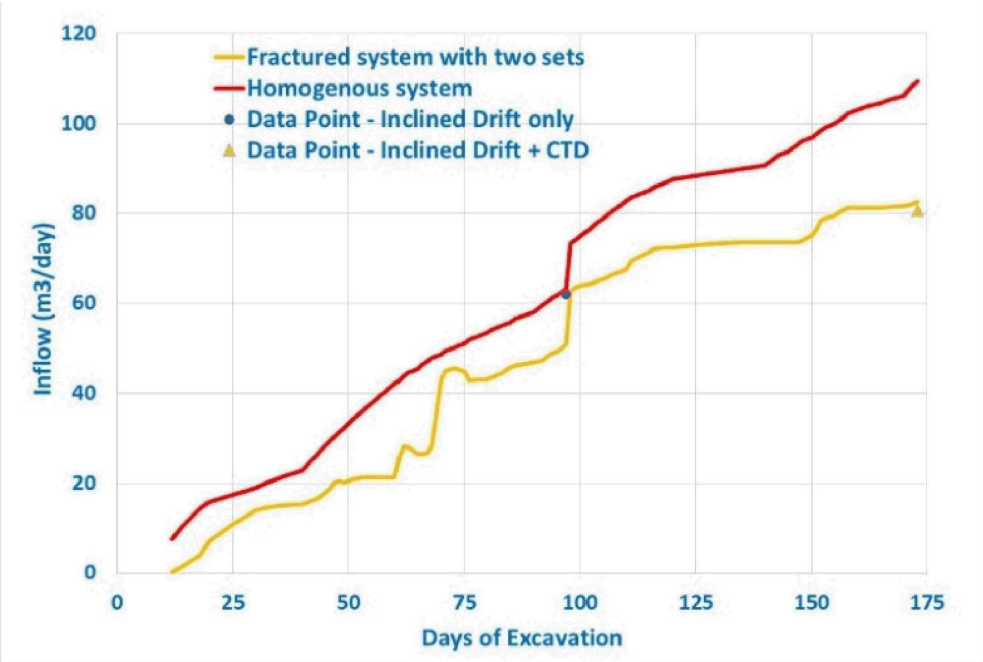

Fig. 4-9: Predicted and observed inflows into Inclined Drift and CTD.

4.4 SUMMARY

This analysis demonstrated an approach to developing a small-scale discrete fracture network model around the Research tunnel. The data used included fracture traces mapped on the tunnel walls, fractures observed in borehole 12MI33, packer test results in 6 test intervals of borehole 12MI33, and measured inflow into the different segment of the Research tunnel during the tunnel excavation.

The DFN model includes:

(1) The fractures observed in the Research tunnel and borehole 12MI33. These fractures have deterministic locations and stochastic (radius, permeability, and aperture) properties derived from the fracture analysis.
(2) Stochastic fractures (the location changes with each realization) generated based on the fracture size, orientation, intensity, and properties derived from the fracture analysis.

The DFN model was upscaled to an effective continuum model for flow and transport simulations. The effective continuum model was capable to predict the observed inflows into the tunnel.

4.5 REFERENCES

Ando, K., Tanaka, T., Hashimoto, S., Saegusa, H., and H. Onoe. 2012. Study for establishment of the methodology for hydrogeological modeling using hydraulic discrete fracture networks (study on hydrogeology in crystalline fractured rock), *JAEA-Research* 2012-022.

Bruines, P., Tanaka, T., Abumi, K., Hashimoto, S., Saegusa, H., Onoe, H., and M. Ishibashi. 2014. Development and Application of the GeoDFN and HydroDFN at the Mizunami Underground Research Laboratory, *8th Asian Rock Mechanics Symposium, October 14-16.* Sapporo, Japan.

Butscher, C. 2012. Steady-State Groundwater Inflow into a Circular Tunnel, *Tunnelling and Underground Space Technology.* 32, 158–167.

Golder Associates, Inc. 2017. Interactive Discrete Feature Data Analysis, *Geometric Modeling and Exploration Simulation, FracMan Manual.* April 6.

Hadgu, T, E.A. Kalinina, Y. Wang, Y. Ozaki, and T. Iwatsuki. 2018. Investigations of Fluid Flow in Fractured Crystalline Rocks at the Mizunami Underground Research Laboratory. In *Proceedings of the 2nd International Discrete Fracture Network Conference, June 20-22, 2018*. Seattle, Washington.

Hammond, G.E., P.C., Lichtner, and R.T., Mills. 2014. Evaluating the Performance of Parallel Subsurface Simulators: An Illustrative Example with PFLOTRAN. *J. Water Resources Research*. 50, doi:10.1002/2012WR013483.

Iwatsuki, T.R., R. Furue, H. Mie, S. Ioka, and T. Mizuno. 2005. Hydrochemical baseline condition of groundwater at the Mizunami underground research laboratory (MIU). *J. Applied Geochemistry*. 20(12): 2283–2302.

Iwatsuki, T., H. Hagiwara, K. Ohmori, T. Munemoto, and H. Onoe. 2015 Hydrochemical disturbances measured in groundwater during the construction and operation of a large-scale underground facility in deep crystalline rock in Japan. J. *Environmental Earth Sciences*. 74(4): 3041-3057.

5. INVESTIGATIONS OF FLUID FLOW IN FRACTURED CRYSTALLINE ROCKS AT THE MIZUNAMI UNDERGROUND RESEARCH LABORATORY

5.1 INTRODUCTION

Characterization of the natural system is of importance to geologic disposal of nuclear waste. The Mizunami Underground Research Laboratory, located in Tono area (Central Japan), is a research facility administered by the Japan Atomic Energy Agency (JAEA). The facility provides scientific basis for the research and development of technologies needed for deep geological disposal of radioactive waste in fractured crystalline rocks. Further description of the hydrogeology of the area can be found in Iwatsuki et al., 2005 and Iwatsuki et al., 2015. Fig. 5-1 shows location and details of the research facility. The part of the tunnel where the modeling is based is given in Fig. 5-2, showing the Inclined Drift, Closure Test Drift (CTD) sections of the tunnel. The figure also shows a monitoring well (12MI33) together with monitoring locations in the well. Through the Development of Coupled Models and their Validation against Experiments (DECOVALEX19) project, a comprehensive set of fracture, hydrologic and chemical data were obtained based on experiments in a research tunnel located at 500 m depth. Development of a discrete fracture network (DFN) model is presented in the previous section of this report. Section 4 describes the fracture model development based on fracture data collected from the excavated areas and boreholes. The fracture data analysis produced upscaled permeability and porosity data for flow and transport modeling. In generating the permeability and porosity fields the matrix rock was assigned a permeability of 10^{-19} m^2 and a porosity of 0.001. In this study, the focus is on flow analysis near the research tunnel using the upscaled fracture model.

The aim of this section is to predict the amount of inflow into the research tunnel as the tunnel sections are excavated. The simulation also aims to provide pressure histories at selected monitoring locations (shown in Fig. 5-2) due to the excavation process. Flow simulations were conducted with PFLOTRAN (Hammond et al., 2014), an open source, state-of-the-art massively parallel subsurface flow and reactive transport code in a high-performance computing environment.

The project provided data of tunnel excavation progress, as tunnel sections are excavated is shown in Fig. 5-3. The figure shows excavation progress in terms of days since excavation began. The excavation data have been used in simulations of inflow into the tunnel.

The excavation progress was modeled by progressively removing material assigned as the host rock. This is equivalent to increasing the grid blocks representing the tunnel as a function of time. To get a better representation of the excavation progress, a small portion of rock material was removed at a time. Thus, the material removal was in 1 m increments for a total of 103 m tunnel length. This resulted in 103 PFLOTRAN runs applying the pressure boundary conditions assigned for the excavated area. The modeling was carried out with output of each PFLOTRAN run used as input for the next run until the complete excavation of the tunnel parts was complete. Thus, the first PFLOTRAN run uses the steady state output representing the specified initial conditions, while the rest of the 103 PFLOTRAN runs uses transient starting points. To automate the simulation process, the optimization code, DAKOTA (Adams, et al., 2017) was used as a driver to PFLOTRAN.

Simulations were carried out for a homogenous representation using the site-scale domain. These simulations are detailed in Section 5.2.1. Simulations were also conducted for a fracture system and are described in Section 5.2.2. Discussion of results and conclusions are given in Section 5.3.

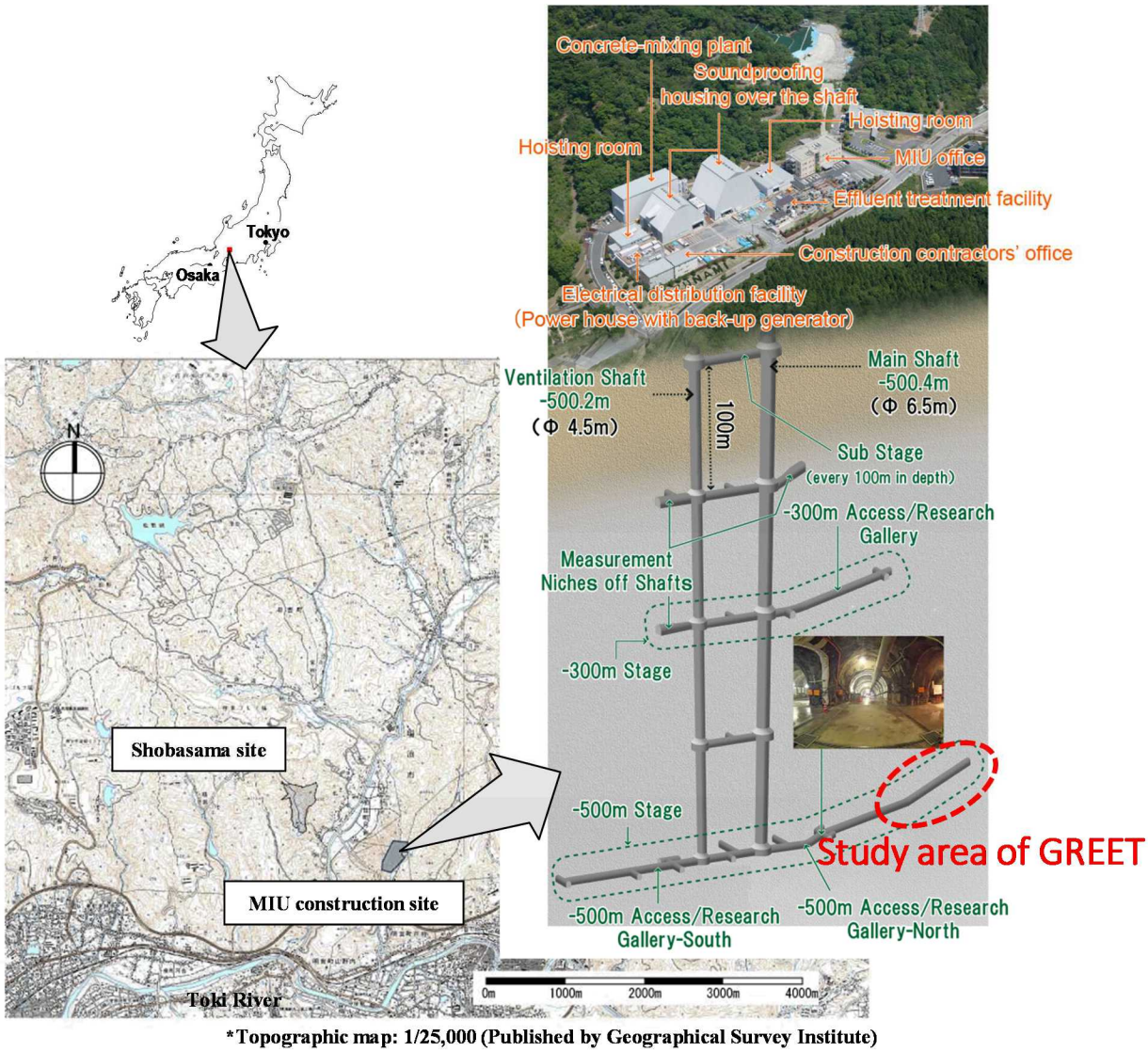

Fig. 5-1: Location and layout of the Mizunami Underground Research Laboratory.

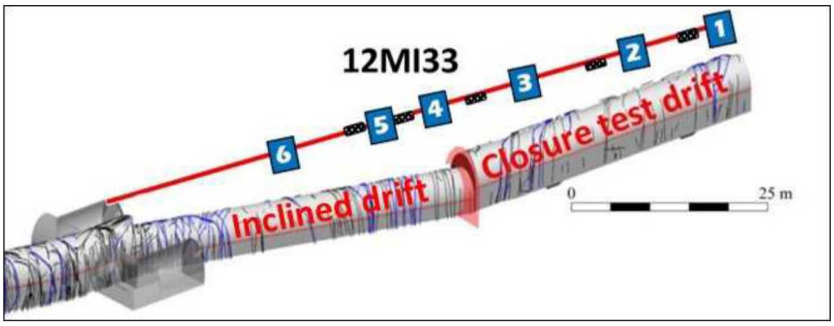

Fig. 5-2: Schematic diagram showing the modeled part of the tunnel and monitoring well 12MI33 with monitoring sections.

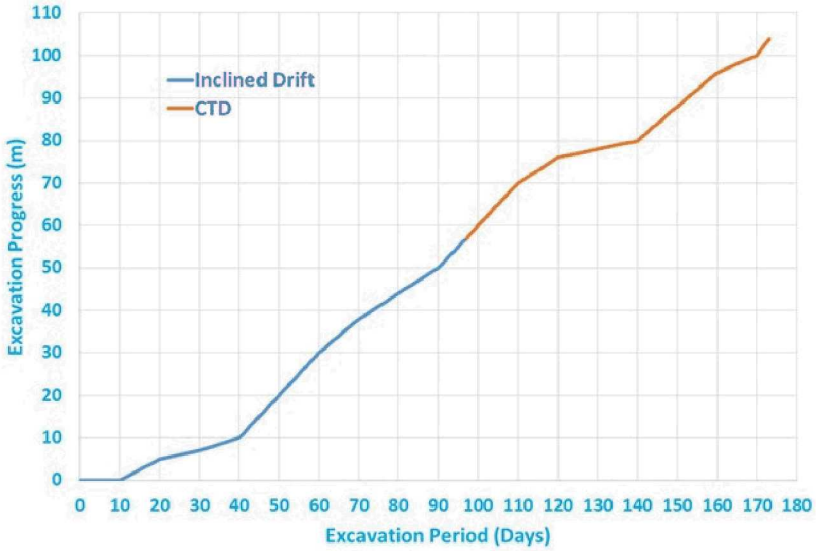

Fig. 5-3. Data of tunnel excavation progress.

5.2 MODEL SETUP

Simulations were based on a site-scale domain with a geometry of 100 m x 150 m x 100 m in the x, y and z directions, respectively. The modeling domain incorporates the Inclined Drift and the CTD sections of the tunnel with dimensions given in Table 5-1. Figure 5-4 shows placement of the tunnel in the modeling domain. The simulation domain also incorporates the monitoring sections in Well 12MI33. For the simulations, a refined Uniform (structured) grid was selected, with grid block size of 1 m x 1m x 1m for a total of 1,500,000 grid blocks.

Table 5-1: Dimensions of the tunnel sections

	Inclined Drift	CTD
Length (m)	57	46.5
Width (m)	4.5	5.0
Height (m)	3.5	4.5

Initial and boundary conditions were based on project specified data. Hydrostatic initial pressure conditions are represented by average head measurements of 110 m, based on data from monitoring wells. Top, bottom and side boundary conditions were also assigned head of 110 m. The excavated area was assigned a constant pressure boundary condition of 1.0 atmosphere. Head data were converted to hydrostatic pressure using the head of 110 m and elevation data for specific locations. Thus, the pressure at the top and bottom of the simulation domain were calculated to be 3.6 MPa (using elevation of -250 m) and 4.6 MPa (using elevation of -350 m), respectively. Hydrostatic pressure boundary condition was assigned on the sides of the domain.

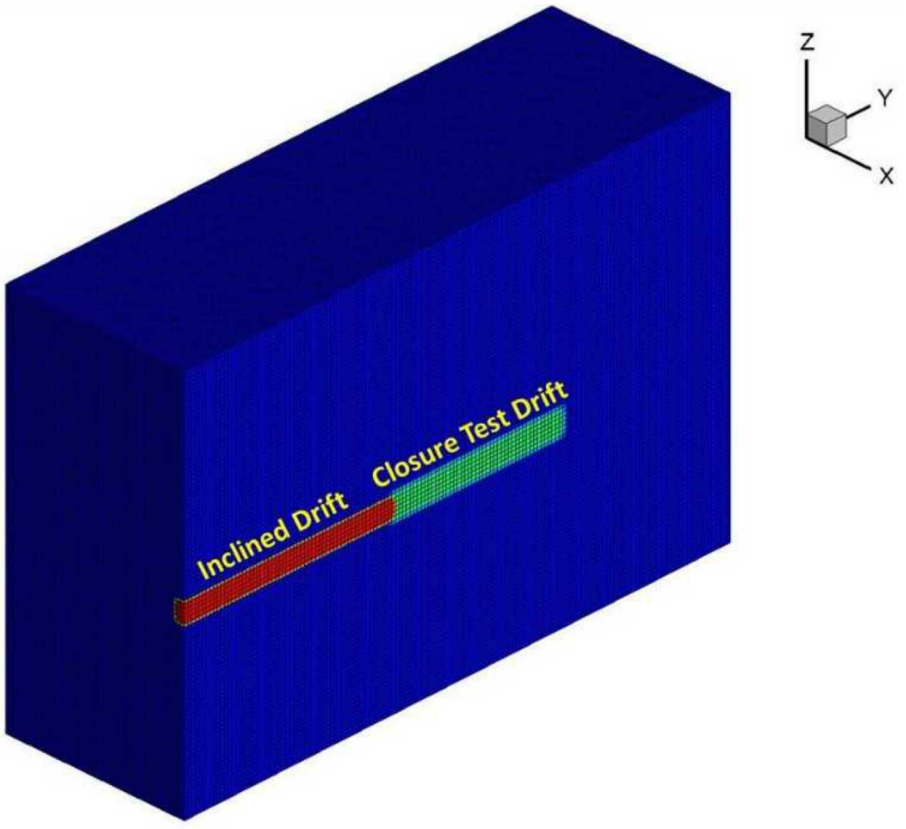

Fig. 5-4: Representation of the tunnel in the modeling domain

5.2.1 Homogenous System Flow Model

Simulations were first conducted for a homogenous model with reference hydraulic conductivity. For the simulations, physical properties obtained from the monitoring well 12MI33 and other sources were used. Estimated hydraulic conductivity for Toki granite is in the range of log (-8 ± 1) m/s. The homogenous simulations used a constant reference hydraulic conductivity of 10^{-8} m/s (permeability 10^{-15} m^2) and a porosity of 0.001. Initial and boundary conditions described above were applied. A steady state run was made to obtain initial pressure conditions in the model domain before the excavation progress was modeled. Simulations of excavation progress were conducted using the steady state pressure distributions and the constant pressure boundary condition inside the tunnel. The DAKOTA-PFLOTRAN system described above was used to separately model excavation progress in the Inclined Drift and the CTD. The outputs were post-processed to evaluate inflow into the tunnel and pressure history at the observation points. The flow of water into the excavated space (Inclined Drift and CTD) was predicted based on the excavation progress. Results of pressure distribution at simulation time of 173 days are shown in Fig. 5-5. The figure represents fluid flow into the tunnel due to the initial and boundary conditions. The fluid movement represents the assumed isotropic system. Fig. 5-6 shows predicted pressure vs. time at the selected monitoring points (see Fig. 5-2 for locations of the monitoring points). Higher pressure drawdown is predicted in Observation Section 6, which is closer to the Inclined Drift entrance. The lowest predicted pressure drawdown is in Section 1, which is close to the edge of the CTD. This is in line with expectations as the inclined tunnel was open for a longer time than the CTD, and thus observation sections close to the Inclined Drift would show more pressure drawdown.

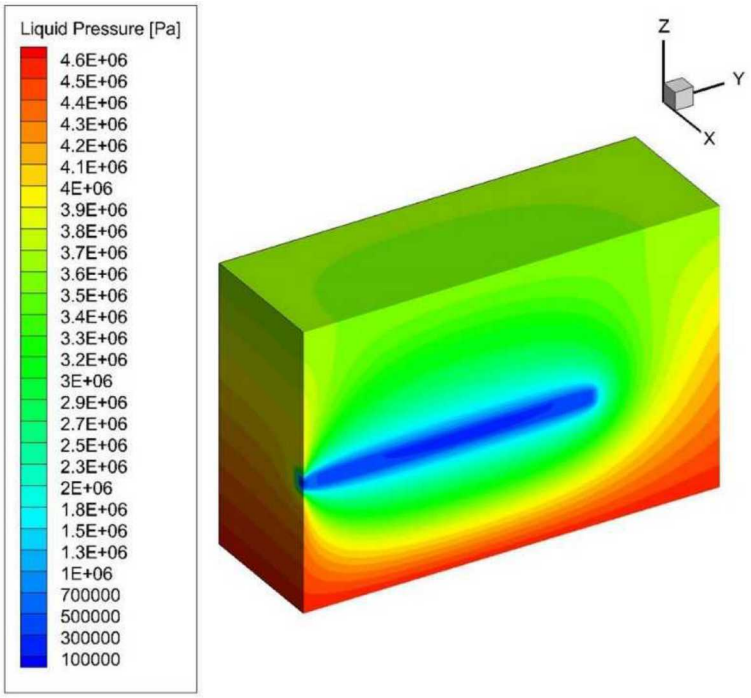

Fig. 5-5: Predicted pressure distribution along tunnel axis after 173 days simulation time: Homogenous Model.

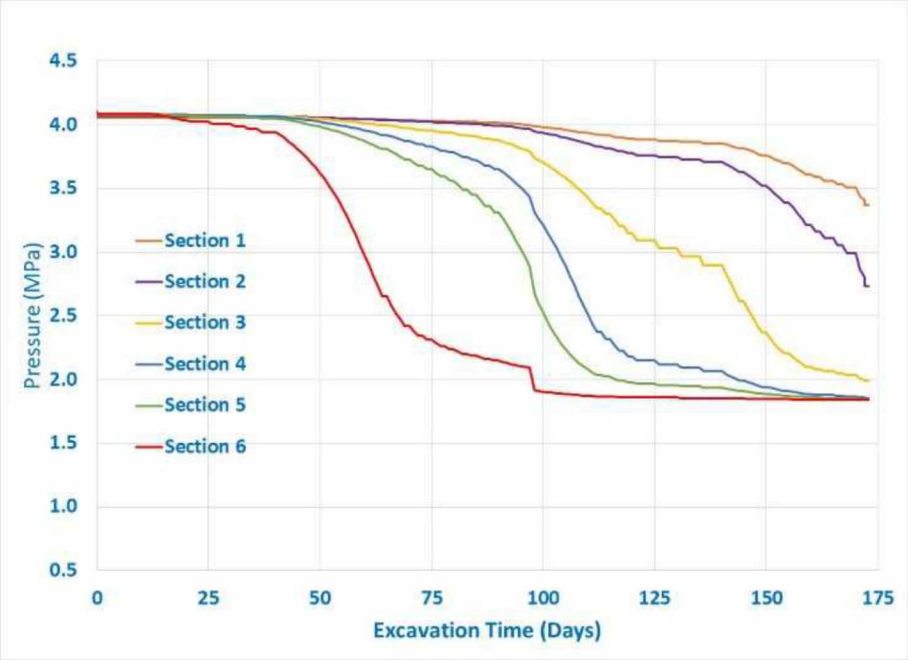

Fig. 5-6: Predicted pressure history at observation points in Well 12MI33 during excavation: Homogenous Model.

5.2.2 Fractured System Flow Model

A single realization with two fracture sets was used for flow simulations using the fracture model. Table 2 shows properties of the two fracture sets produced from the fracture model development described in the companion paper by Kalinina et al., 2018. Fig. 7 shows representation of transmissivity for a DFN model realization (Kalinina et al., 2018). Figs. 8 and 9 show the upscaled permeability and porosity fields for the realization used in numerical modeling of flow.

Table 5-2: Fracture orientation distributions

Fracture Set	Trend (^{0})	Plunge (^{0})	Fisher Dispersion k	Volumetric Intensity P_{32} (1/m)
Set 1	208	8	7	0.22
Set 2	303	1.3	3.6	0.086

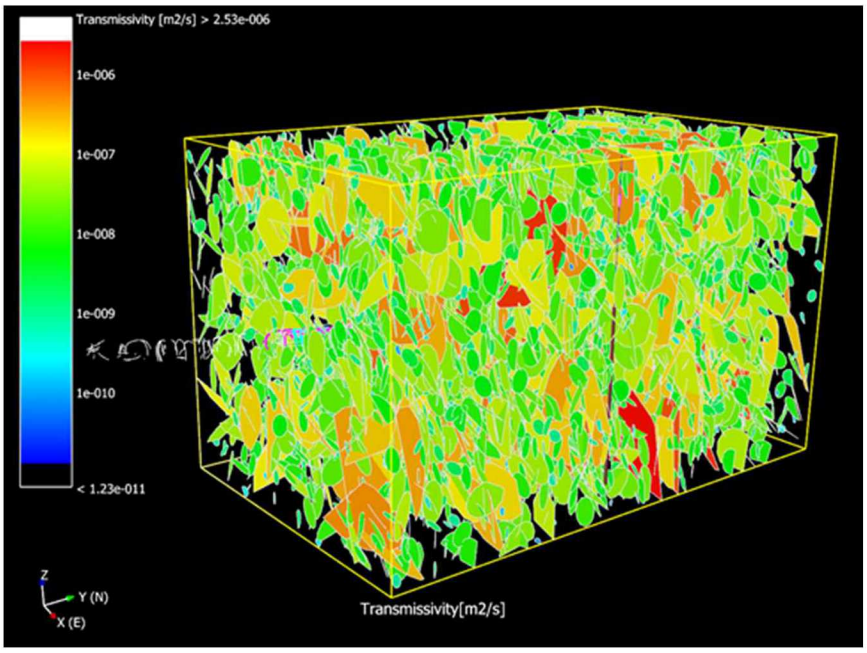

Fig. 5-7: Transmissivity of a realization of the discrete fracture network: Fracture Model

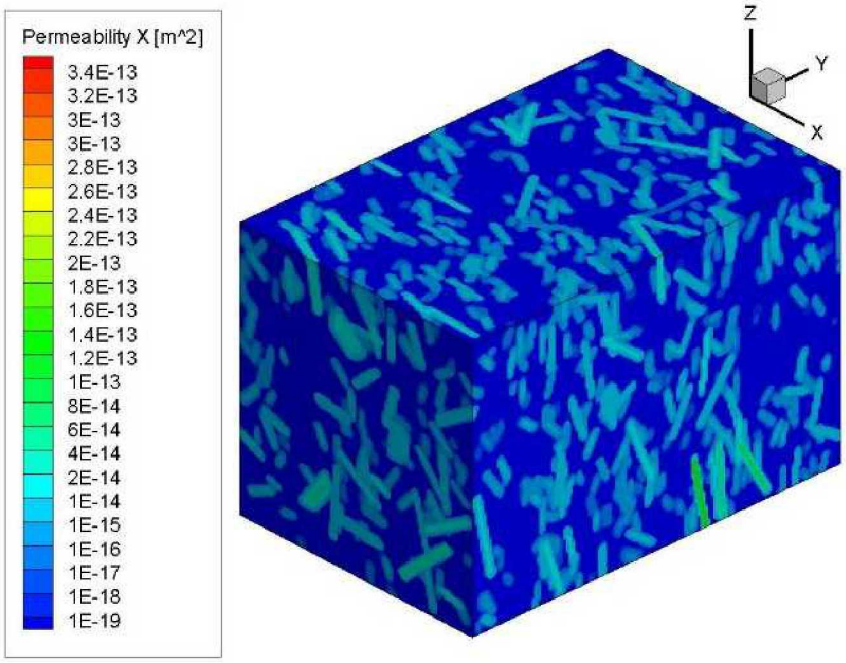

Fig. 5-8: Upscaled permeability: Fracture Model

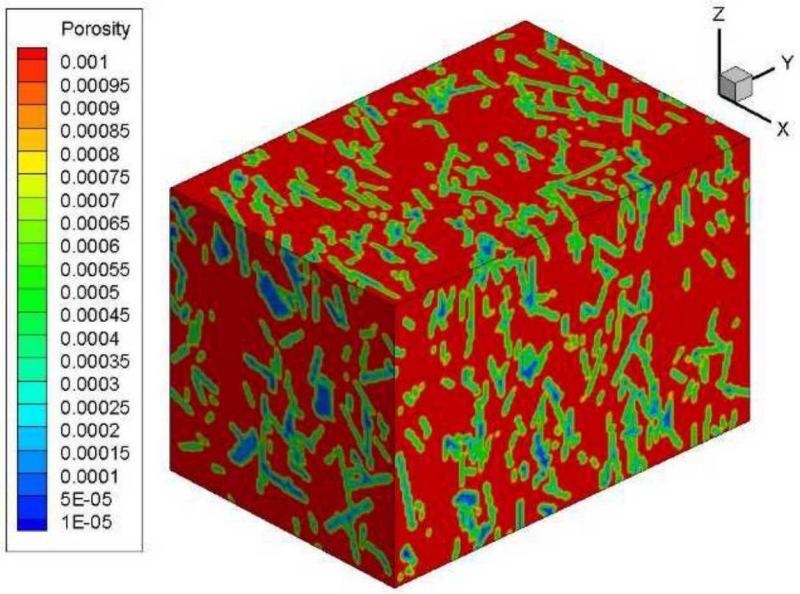

Fig. 5-9: Upscaled porosity: Fracture Model

Flow-based effective permeability representing the entire fractured rock domain was calculated using Darcy's law and liquid flux at steady state. Flow simulations were carried out using the upscaled permeability and porosity fields to estimate the flow-based effective permeability. A pressure gradient was imposed between the west and east faces of the simulation domain. The resulting calculated effective permeability along the x-axis (perpendicular to tunnel axis) for the fracture realization was 3.27 x 10^{-16} m^2, which less than the isotropic permeability used for the homogenous model by a factor of 0.327. Flow-based effective permeability values were also calculated for flow in the other directions. The complete results are shown below. The effective permeability in the vertical direction is higher than the horizontal values, indicating more flow in the vertical direction.

- Horizontal flow, perpendicular to the tunnel axis (x-axis), effective permeability: 3.27 x 10^{-16} m^2
- Horizontal flow, along the tunnel axis (y-axis), effective permeability: 1.95 x 10^{-16} m^2
- Ratio of horizontal flow effective permeability y-axis/x-axis: 0.6
- Vertical flow (z-axis), effective permeability: 5.14 x 10^{-16} m^2
- Ratio of effective permeability z-axis/x-axis: 1.6

The simulation procedure for the homogenous model described in Section 5.2.1, using the coupled DAKOTA-PFLOTRAN codes, was also applied to the fractured system simulation runs. Simulation results for the fractured system are shown in Figs. 5-10 to 5-12. Fig. 5-10 shows pressure distributions at 173 days simulation time. The pressure distribution indicates flow into the tunnel in a fractured system along the axis of the tunnel. Predictions of pressure at observation points are shown in Fig. 5-11. The pressure drawdown for most of the observation sections are higher than those of the homogenous model because the heterogenous character of the fracture model plays an important role.

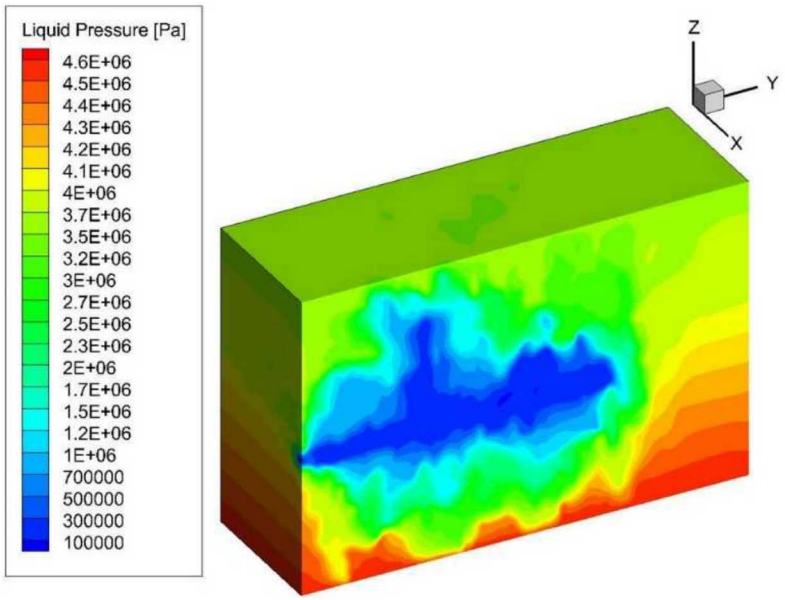

Fig. 5-10: Predicted pressure distribution along tunnel axis after 173 days simulation time: Fracture Model

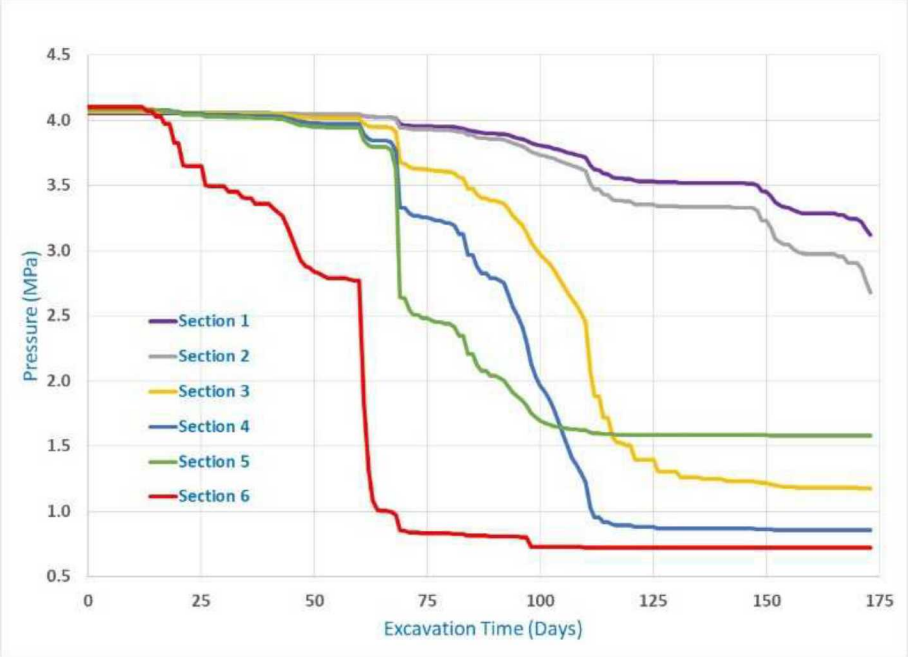

Fig. 5-11: Predicted pressure history at observation points in Well 12MI33 during excavation: Fracture Model.

The flow of water into the excavated space was also evaluated for the fractured system. The resulting predictions of inflow into the tunnel is shown in Fig. 4-9 together with the results for the homogenous model. Project inflow experimental data points are also included. The predicted inflow for the homogenous model matches the experimental inflow to the Inclined Drift, but over predicts the inflow to the CTD. The predicted inflow for the fracture model matches both experimental data points. Note that the above results are for a single fracture model realization. A better representation would be obtained when results are

averaged over an adequate number of realizations. Further modeling will include generation of a representative sample of realizations.

5.3 CONCLUSIONS

Preliminary modeling analysis was conducted to predict inflow of water during excavation of the Inclined Drift and CTD section of the tunnel at the Mizunami Underground Laboratory, as part of DECOVALEX19 study. The analysis looked at the use of a homogenous model with reference hydraulic conductivity, and a fracture model developed by Kalinina et al. 2018. The simulations used a site-scale domain of size 100 m x 150 m x 100 m. Boundary and initial conditions specified by the project, based on data from wells, were applied to flow simulations. Parameter data also obtained from wells were used. Data of excavation progress for the Inclined Drift and the CTD were also provided.

The modeling analysis using the homogenous model provided a simpler isotropic representation of the porous medium. However, simulation results showed uniform fluid flow and thus the model was not able to capture local hydrologic variations. The modeling analysis using the fracture model with upscaled permeability and porosity fields allowed realistic representation of the hydrology of the fractured rock in the excavated region. The simulation results provided detailed flow analysis in a fractured system. The predicted inflow of the realization with two fracture sets matched the experimental data. The results are preliminary output for a single fracture realization. More realizations will be needed to obtain average representative output.

5.4 REFERENCES

Iwatsuki, T.R., R. Furue, H. Mie, S. Ioka, and T. Mizuno. 2005. Hydrochemical baseline condition of groundwater at the Mizunami underground research laboratory (MIU). *J. Applied Geochemistry*. 20(12): 2283–2302.

Iwatsuki, T., H. Hagiwara, K. Ohmori, T. Munemoto, and H. Onoe. 2015 Hydrochemical disturbances measured in groundwater during the construction and operation of a large-scale underground facility in deep crystalline rock in Japan. J. *Environmental Earth Sciences*. 74(4): 3041-3057.

Kalinina, E, T. Hadgu, Y. Wang, Y. Ozaki, and T. Iwatsuki. 2018. Development and Validation of a Fracture Model for the Granite Rocks at Mizunami Underground Research Laboratory, Japan, *in Proceedings of the 2nd International Discrete Fracture Network Conference, Seattle, Washington*, June 20-22, 2018.

Hammond, G.E., P.C., Lichtner, and R.T., Mills. 2014. Evaluating the Performance of Parallel Subsurface Simulators: An Illustrative Example with PFLOTRAN. *J. Water Resources Research*. 50, doi:10.1002/2012WR013483.

Adams, B. M. et al. 2017. Dakota, A Multilevel Parallel Object-Oriented Framework for Design Optimization, Parameter Estimation, Uncertainty Quantification, and Sensitivity Analysis: Version 6.6 User's Manual. SAND2014-4633. Updated May 9, 2017.

5. SUMMARY

SNL has been participating in three tasks of the DECOVALEX project: Task A. Modeling gas injection experiments (ENGINEER), Task C. Modeling groundwater recovery experiment in tunnel (GREET), and Task F. Fluid inclusion and movement in the tight rock (FINITO). FY18 work focused on Task C. The major accomplishments are summarized below:

- *Task A. Modeling gas injection experiments (ENGINEER):* Bentonite has been proposed as a buffer material for a deep geologic repository. Understanding gas migration in compacted clay materials is important for a performance assessment of an engineered barrier system of a repository system. Existing data demonstrate the complexity of gas migration in such low-permeability materials. Through a time-series analysis of outflow rate, we show that gas migration in water saturated compacted clay material exhibits a typical deterministic chaotic behavior. The dimension of the system ranges from 3 to 4. The dynamic behavior of the system has been shown closely related to clay matrix dilation, fracturing and fracture healing as induced by gas bubble movement. The concept proposed here provide a new perspective for modeling gas migration in low-permeability materials.
- *Task C. Modeling groundwater recovery experiment in tunnel (GREET):* The task uses the data collected in a research tunnel at 500 m depth, at the Japan Atomic Energy Agency (JAEA) Mizunami Underground Research Laboratory (MIU), to understand the hydrological-mechanical-chemical environment. The model analysis conducted in FY18 has demonstrated a general approach to developing a small-scale discrete fracture network model around the Research tunnel. The data used included fracture traces mapped on the tunnel walls, fractures observed in borehole 12MI33, packer test results in 6 test intervals of borehole 12MI33, and measured inflow into the different segment of the Research tunnel during the tunnel excavation. The discrete fracture network (DFN) model includes:
    a. The fractures observed in the Research tunnel and borehole 12MI33. These fractures have deterministic locations and stochastic (radius, permeability, and aperture) properties derived from the fracture analysis.
    b. Stochastic fractures (the location changes with each realization) generated based on the fracture size, orientation, intensity, and properties derived from the fracture analysis.

  The discrete fracture network model was then upscaled to a continuum model to be used in flow simulations. A flow model was developed centered on the research tunnel, and using a highly refined regular mesh. In this study development and utilization of the model is presented. The modeling analysis used permeability and porosity fields from the discrete fracture network model as well as a homogenous model using fixed values of permeability and porosity. The simulations were designed to reproduce hydrology of the modeling area and to predict inflow of water into the research tunnel during excavation. Modeling results were compared with the project hydrology data. Successful matching of the experimental data was obtained for simulations based on the discrete fracture network model.
- *Task F. Fluid inclusion and movement in the tight rock (FINITO):* Fluid inclusions can be found within mineral crystals or along grain boundaries in all types of sedimentary rocks. For a long-term performance assessment of a geologic repository, it is important to characterize the distribution, amount and interconnectivity of fluid inclusions in the host rock and to predict migration of these inclusions after waste emplacement. Task F is designed to gain mechanistic understanding of possible physical processes involved in fluid inclusion migration in tight rocks such as rock salt, with an ultimate goal to develop robust, predictive THMC modeling tools for a long-term performance assessment of a deep geologic repository in such media. The task will leverage the data provided by BGR, Germany. In fiscal year 2018, the work at SNL has refined the model for individual fluid inclusion migration in rock salt. The model developed can qualitatively explain a number of key features of experimental observations. Specifically, the

model can predict: (1) a linear increase in migration evelocity with increasing thermal gradient, (2) a nonlinear increase in migration velocity with inclusion size, (3) an overall aceleration in fluid migration with temperature, (4) the dependence of migration velocity on mechanical loadings. A preliminary analysis for biphase fluid inclusions has also been performed. A bifurcation point in vapor/liquid volume ratio for the direction of fluid migration is derived.